INTERMOLECULAR INTERACTIONS IN COMPRESSED CRYSTALS

Damian Paliwoda

A DISSERTATION SUBMITTED TO
THE ADAM MICKIEWICZ UNIVERSITY IN POZNAŃ
IN PARTIAL FULFILLMENT OF THE REQUIREMENTS
FOR THE DEGREE OF DOCTOR OF PHILOSOPHY

SUPERVISOR: Prof. Dr. hab. Andrzej Katrusiak
ASSISTANT SUPERVISOR: Dr. Kamil Dziubek

Poznań, February 2014

INNOVATIVE ECONOMY
NATIONAL COHESION STRATEGY
ADAM MICKIEWICZ UNIVERSITY IN POZNAŃ
FNP Foundation for Polish Science
EUROPEAN UNION

ODDZIAŁYWANIA MIĘDZYCZĄSTECZKOWE W KRYSZTAŁACH POD WYSOKIM CIŚNIENIEM

Damian Paliwoda

PRACA WYKONANA W ZAKŁADZIE CHEMII MATERIAŁÓW
I PRZEDSTAWIONA RADZIE NAUKOWEJ WYDZIAŁU CHEMII
UNIWERSYTETU IM. ADAMA MICKIEWICZA W POZNANIU
CELEM UZYSKANIA STOPNIA NAUKOWEGO
DOKTORA NAUK CHEMICZNYCH

PROMOTOR: prof. dr hab. Andrzej Katrusiak
PROMOTOR POMOCNICZY: dr Kamil Dziubek

Poznań, Luty 2014

INNOVATIVE ECONOMY
NATIONAL COHESION STRATEGY
ADAM MICKIEWICZ UNIVERSITY IN POZNAŃ
FNP Foundation for Polish Science
EUROPEAN UNION

Acknowledgements

I am greatly indebt to my supervisor Prof. Andrzej Katrusiak and assistant supervisor Dr. Kamil Dziubek. Professor Andrzej Katrusiak gave me an opportunity to participate in the doctoral fellowship in Poznań. I would like to express my sincere appreciation to him for his invaluable assistance during the course of this project, endless enthusiasm and long-lasting, stimulating discussions.

Many thanks for Dr. Kamil Dziubek, for his guidance in high-pressure techniques, performing calculations, which are included in my thesis, and for a number of valuable remarks.

I would like to express my sincere appreciation to Ms. Katarzyna Kowalska and Dr. Michael Hanfland from European Synchrotron Radiation Facility for performing high-pressure diffraction experiments on ferrocene crystals.

A big thank you to Ms. Paulina Wawrzyniak, who worked with me on the high pressure studies of gold compounds for her great support and constant encouragement.

Finally, I would also like to thank all of my colleagues and co-workers from Professor Katrusiak's group for friendly atmosphere and fruitful discussions in the laboratory.

„The best way to have a good idea is to have lots of ideas."

Linus Pauling

Financial support from the TEAM programme of the Foundation for Polish Science, TEAM 2009-4/6, is gratefully acknowledged.

Contents

1

Introduction

Pressure is one of basic thermodynamic parameters, however its effect on chemical reactions, properties of materials and their structure remains relatively poorly understood, mainly due to the lack of experimental data. This deficiency of high-pressure information, compared to the vast amount of low- and high-temperature data, is due to the technical requirements of high-pressure experiments. They could be conducted only in strong vessels with thick walls, capable of withstanding high pressure, but obscuring access to the sample. The breakthrough in the high-pressure methods was the invention of the diamond-anvil cell, DAC (Weir *et al.,* 1959). Its design evolved in the second half of XXth century and finally made the DAC a powerful tool for *in situ* spectroscopic and diffraction investigations.

Initially, high-pressure techniques were applied mainly for geological and geophysical studies. Later, they have also been used in chemical and physical laboratories, in order to investigate properties, high-pressure behaviour and phase transitions of elements, small-molecule compounds and macromolecular structures, such as proteins. Pressure is also used for obtaining new functional materials and for modifying their properties. Still today, little is known about effects of pressure on molecular structure, conformation and intermolecular interactions. A number of fascinating results in this field have been reported over last decades (Boldyreva, 2008).

Polymorphism of elements is one of the most intriguing phenomena. At 39 GPa metallic lithium undergoes a phase transition to the semi-metallic cubic polymorph (Hanfland *et al.,* 2000). Moreover, simple compounds at high pressure turn out to be not so-simple anymore. Most recently new stoichiometries of sodium chloride were predicted under high pressure. Two of them, stable at high pressure, $NaCl_3$ and two-dimensional metallic Na_3Cl were synthesized (Zhang *et*

al., 2013). Several interesting examples of pressure-induced crystallizations of liquids, such as benzene, carbon disulphide, halomethanes, have been also described (Bridgman, 1914; Katrusiak *et al*., 2010; Dziubek & Katrusiak, 2004; Bujak *et al*., 2008). These experiments confirmed that despite preserving the molecular structure at high pressure, these compounds acquire new properties, different than in normal conditions.

The aims of this dissertation includes high-pressure structural determination of intermolecular interactions and phase transitions in selected organic and hybrid inorganic-organic materials.

Due to the increasing interest in highly stable and environment-friendly materials with giant dielectric response, ferroelectrics and relaxors, I have engaged into the studies of pressure-induced transformations of switchable NH···N hydrogen bonds in organic crystals. For this purposes one of the simplest and prototypic molecular NH···N-bonded compounds was chosen (*Figure 1*). Its prominent role in chemistry and biochemistry has been thoroughly investigated (Burt & Silver, 1973, Yoshizawa *et al.*, 2001). Imidazole takes part in biochemical processes and is a component of active sites of many enzymes, such as catalytic triad and zinc containing alcohol dehydrogenase. In the solid state imidazole forms monoclinic crystals, where molecules are NH···N hydrogen bonded into chain, as shown in *Figure 1*. The crystals of imidazole were intensely studied at varied temperature, however, no solid state transitions were found. A pressure-driven transformation of NH···N bonds in imidazole crystals and a unique 'hidden' phase transition are described further in this dissertation.

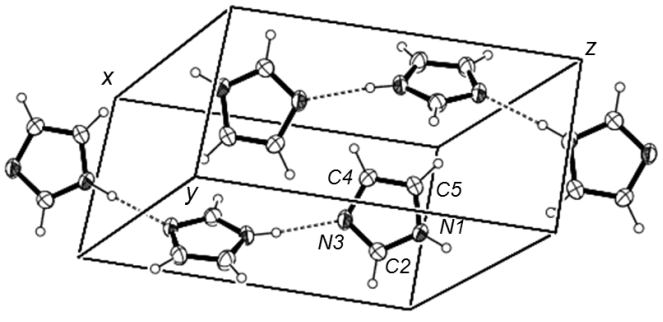

Figure 1. *Molecular arrangement of imidazole molecules in the ambient-pressure crystal. NH···N hydrogen bonds are indicated by dashed lines.*

Another example of unusual behaviour of small-molecule crystals under high pressure is bis(cyclopentadienyl)iron(II), commonly known as ferrocene. Its serendipitous discovery in 1951 initiated the development of organometallic chemistry (Werner, 2012). Because of unclear relative positions cyclopentadienyl rings (*Figure 2*) and their dynamic disorder at ambient conditions, the sandwich-like structure of ferrocene raised questions about its conformation. Combined synchrotron and laboratory X-ray diffraction experiments, as well as Raman spectroscopy, have been performed and described herein in order to explain pressure-induced transformations of ferrocene crystals.

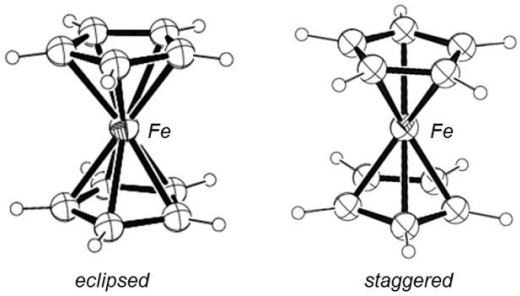

***Figure 2**. Molecular conformations of ferrocene with cyclopentadienyl rings eclipsed (left) and staggered (right).*

Since the late 1980s much attention has been paid to the chemistry of gold coordination compounds (Schmidbaur, 2000). The aurophilic phenomenon, described as tendency of gold atoms or ions to bind *via* weak interactions between, were observed in gold(I) complexes. Materials with these structural motifs show many interesting luminescent properties. One of such compounds is gold(I) diethyldithiocarbamate, $[AuEt_2DTC]_2$, built of helical Au···Au bonded chains and stabilized by *S*-donor ligands. Its strong pressure-dependent luminescence attracted my attention. I have soon found that low-temperature and high-pressure results are in some points inconsistent with previous reports on gold(I) diethyldithiocarbamate polymer.

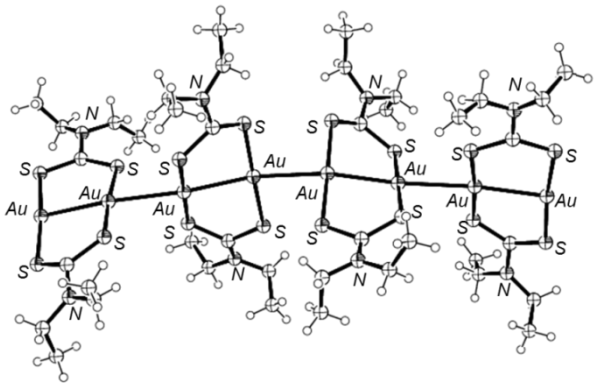

***Figure 3**. Single chain of Au···Au bonded gold(I) diethyldithiocarbamate polymer.*

This dissertation is divided into three separate parts and includes a brief description of the transformations of imidazole, ferrocene and ligand-supported gold(I) polymer under high pressure. Details of these projects have been reported in three publications attached in Appendix A:

A.1

D. Paliwoda, K. Dziubek, A. Katrusiak, Imidazole hidden polar phase, *Cryst. Growth Des.* **2012**, *12*, 4302-4305.

A.2

D. Paliwoda, K. Kowalska, M. Hanfland, A. Katrusiak, U-Turn compression to a new isostructural ferrocene phase, *J. Phys. Chem. Lett.* **2013**, *9*, 4034-4039.

A.3

D. Paliwoda, P. Wawrzyniak, A. Katrusiak, Unwinding Au···Au bonded filaments in ligand-supported gold(I) polymer under pressure**,** *submitted*.

2

High-pressure chemistry

Like temperature, pressure is the thermodynamic parameter efficiently controlling physical processes and chemical reactions. However, the pressure effects on chemical reactions carried out in solution are usually neglected. The parameter that correlates high pressure kinetic experiments in solution is the volume of activation ($V^{\neq}$), defined as the difference between the partial molecular volume of the activated complex and the sum of the partial volumes of the reactants (Laidler, 1996). For reversible reactions $V^{\neq}$ can be replaced by the reaction volume, $V°$, which is correlated with the equilibrium constant (K). It is expressed as:

$$\left(\frac{\partial \ln K}{\partial p}\right)_{\mathrm{T}} = -\frac{\Delta V°}{\mathrm{RT}}$$

where R is the ideal gas constant, T is the absolute temperature and p denotes pressure.

Below 200 MPa the correlation between ln$K$ and p is almost linear. Hence, the reaction volume is pressure independent. Non-linear correlation above 200 MPa arise from solvent compressibility and implies pressure sensitivity of reaction and activation volume. In general, the chemical reactions carried out under high pressure can be divided into two separate types: transition state reactions and single step reactions without intermediates.

However, volume diagrams depend on the reaction mechanism and its reversibility. The intrinsic changes of bond lengths and angles, as well as solvational effects strongly contribute to the reaction or activation volume. When solvational contributions are neglected, the positive value of activation volume indicates bond breakage, while negative values are characteristic for new bonds formation.

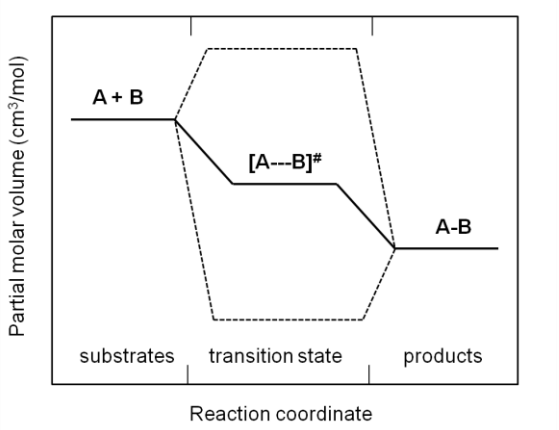

Figure 4. *Volume diagram of the pressure-induced reaction A + B → A-B. The transition state is indicated as [A---B]# (reproduced from van Eldik & Hubbard, 2002).*

Several examples of pressure-induced chemical processes are known and well described. The first one was reported in 1892 by Wilhelm Röntgen. The acid-catalyzed inversion of sucrose were carried out using pressures of 500 bar (Röntgen, 1892). Pressure-induced polymerization of liquid 2-methyl-1,3-butadiene (isoprene) has been reported in 1929 by Bridgman and Conant (Bridgman & Conant, 1929). Nearly a half of century later Rimmelin and Jenner described the Diels-Alder cycloaddition and dimerisation in compressed isoprene (Rimmelin & Jenner, 1974).

A large group of inorganic, organic or hybrid materials can be synthesized in high pressure autoclaves. Many of these materials are porous. The porosity is a highly desired aspect increasing the catalytic activity of the material. This feature of functional materials strongly depends on the solvent-accessible voids size. In general, porous materials can be separated into three classes: nanoporous, microporous and mesoporous. Apart from the micro- and mesoporous silica-based materials, much attention has been devoted to the synthesis of nanoporous metal organic frameworks, MOFs. Pressure-driven supramolecular Ag···Ag bonded argentophilic interactions have been recently characterized in silver 2-methylimidazolate metal organic framework (Ogborn *et al.*, 2012).

Many high-pressure transformations of chemical elements have been reported. At high pressure oxygen undergoes phase transition to the red *ε*-phase. Single crystal X-ray studies performed in the pressure range between 13 and 18 GPa confirmed that four O_2 molecules aggregate into a rhombohedral molecular unit

by forming new, ‘weaker’ chemical bonds (Lundegaard *et al.*, 2006). Eventually, all elements become metallic under high pressure, for example iodine above 16 GPa (Pasternak *et al.,* 1987). On the contrary, one of the most metallic elements, sodium, becomes the transparent insulator at 190 GPa (Ma *et al.*, 2009).

It can be concluded that contemporary chemistry gives many opportunities for using high pressure as an excellent tool for rational design and synthesis of new functional materials with exceptional properties. These chemical opportunities are relatively poorly supported by structural information about materials at high pressure and my thesis was intended to provide new data.

3

High-pressure crystallography

High pressure can be easily generated by squeezing the contents of the chamber in the diamond anvil cell, DAC (*Figure 5*). During the last decades numerous designs of DAC were invented (Jayaraman, 1983; Hazen & Finger, 1982; Eremets, 1996; Besson, 1997; Miletich *et al.*, 2000). In this work a modified Merrill-Bassett diamond anvil cell was used for high-pressure crystallizations and X-ray diffraction experiments (Merrill & Bassett, 1974).

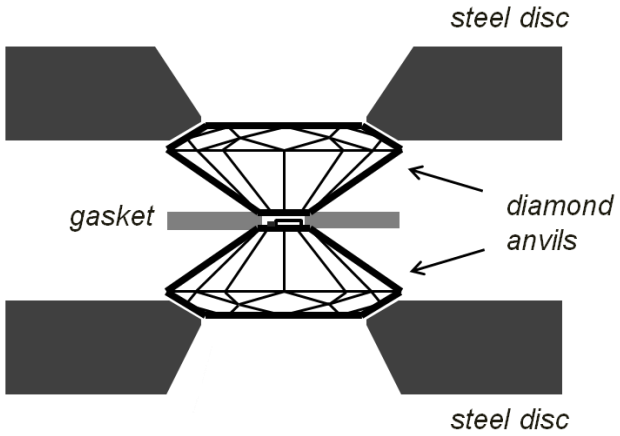

Figure 5. *Schematic view of the main central of a diamond anvil cell (DAC).*

The main part of the DAC are two diamond anvils. This carbon allotrope is the hardest material ever known. Typically two diamond anvils are mounted on beryllium or steel discs (*Figure 6*). However, the beryllium discs are nowadays rarely used because they cause high background and due to the toxicity of beryllium oxide. Furthermore, beryllium softens at about 500 K, which strongly hampers high-temperature experiments (Katrusiak, 2008).

The sample, a small ruby chip for pressure calibration and liquid pressure-transmitting medium are loaded into a miniature reaction chamber, confined between the walls of a spark-eroded hole in the metal gasket and the tips of two

vertically opposed diamonds. In this work, ruby-fluorescence method was used for pressure calibration. The method is based on the red shift of the two narrow bands (692.8 and 694.2 nm at ambient conditions) of ruby fluorescence resulting from the increased pressure. This correlation has been thoroughly investigated and described in the literature (Piermarini *et al*., 1975; Mao *et al*., 1986; Chijioke *et al*., 2005; Syassen, 2008).

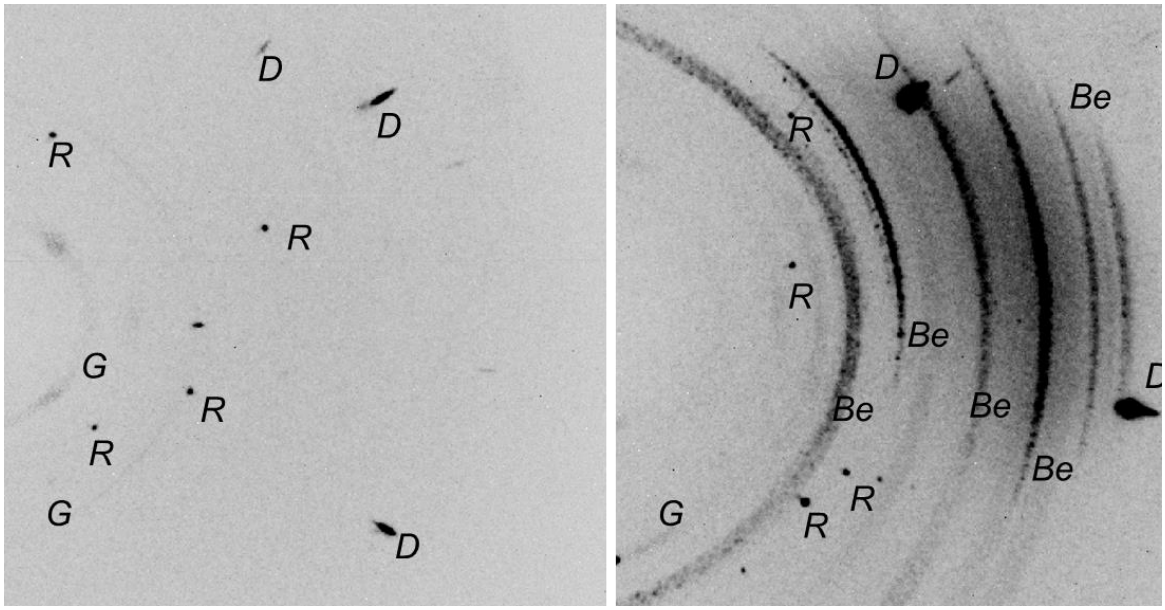

Figure 6. *CCD images of imidazole crystals in a DAC recorded on a KUMA KM4 CCD diffractometer under high pressure. The characteristic feature of diffraction patterns of a DAC with diamonds mounted on steel discs (left) and a DAC with beryllium backing plates (right). The sample-crystal reflections are indicated with letters R, powder rings from the steel gasket (G); beryllium-powder rings (Be); and diamond reflections (D).*

The single-crystal sample can be placed in the pressure chamber in different ways:

(1) it can be glued to the diamond surface (culet), topped by pressure-transmitting medium and closed inside the DAC;

(2) it can be obtained directly in a diamond anvil cell by *in situ* isochoric or isothermal crystallization.

3.1 X-Ray diffraction studies

In this thesis a single crystal KUMA KM4 and Xcalibur Eos diffractometers with a CCD detector and a monochromated Mo sealed-tube source ($K\alpha$ radiation, λ = 0.71073 Å) were used for X-ray single-crystal measurements. For high pressure experiments a gasket-shadow centering alignment procedure of a DAC (Budzianowski & Katrusiak, 2004) was used. The CrysAlisPro program suite was used for data collections, determination of the UB-matrices and initial data reduction. Then the reflection intensities were corrected for the DAC absorption and gasket shadowing and the diamond-anvil reflections were eliminated (Katrusiak, 2003). The structures were solved by using direct methods by program SHELXS and refined by full-matrix least squares with SHELXL (Sheldrick, 2008). H-Atoms were located from the molecular geometry, with the C–H and N–H (for imidazole) distances set to 0.93 and 0.86 A˚, respectively.

4

Polar crystals of imidazole

At ambient and low-temperature conditions, imidazole forms monoclinic crystals, space group $P2_1/c$. Combined piston-cylinder compressibility measurements and high-pressure diffraction studies of imidazole show that it can be compressed in the monoclinic phase to 2.7 GPa at least. However, high-pressure *in situ* recrystallization of imidazole leads its new polar phase, stable above 1.2 GPa.

4.1 NH···N bonded ferroelectrics and relaxors

The most intriguing and characteristic feature of ferroelectric materials is their reversible spontaneous polarization in the presence of external electric field. Non-linear polarization of such systems implies a hysteresis loop (*Figure 7*), is a condition for their application as memory function.

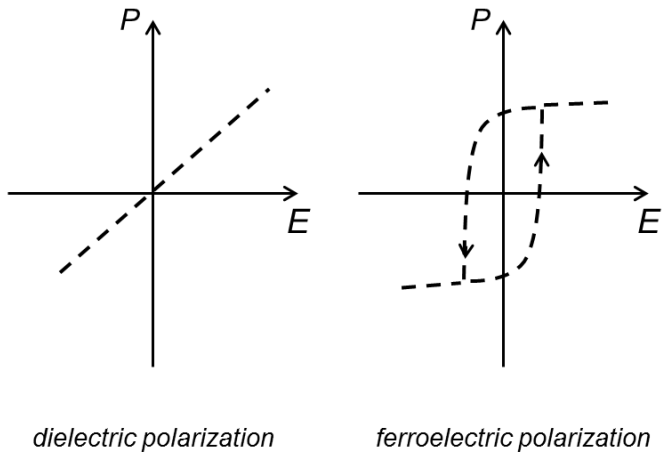

Figure 7. *Dielectric and ferroelectric polarizations (P – polarization, E – external electric field). Hysteresis loop is characteristic for ferroelectric materials.*

Ferroelectric materials are applied in highly efficient and miniaturized capacitors, used in the construction of ferroelectric RAM memories (Scott, 2000).

Still today, a vast majority of ferroelectric materials is based on ionic systems, mainly inorganic salts, such as ceramic perovskites doped with lead. Due to this heavy metal contents, the most serious drawback of these materials is their relatively high toxicity. Hence, their organic substitutes seem to be more green and environment-friendly alternative.

A few examples of switchable, KDP-type (KH_2PO_4; Nazario & Gonzalo, 1969) hydrogen bonded organic ferroelectrics have been reported recently. OH···O bonded croconic acid exhibits ferroelectric behavior (Horiuchi *et al*., 2010). Another type of organic materials include 1,4-diazabicyclo[2.2.2]octane (dabco) monosalts dabcoHX with NH^+···N hydrogen bonds in the structure. Salts with tetrahedral ClO_4^-, BF_4^- and ReO_4^- anions, are ferroelectrics and the ones with small Br^- and I^- anions are stoichiometric anisotropic relaxors (Olejniczak *et al.,* 2010; Szafrański *et al.,* 2010, Szafrański & Katrusiak, 2004).

Compared to the ionic systems, molecular materials can be more advantageous. The NH···N bonded molecular materials, imidazoles and their derivatives, such as pyrazole (Sikora & Katrusiak, 2013), benzimidazole (Zieliński & Katrusiak, 2013) and ferroelectric 2-methylbenzimidazole (Horiuchi *et al.*, 2013) have been described recently.

Liquid imidazole exhibits ionic conductivity, which has been associated with the proton transfer in NH···N bonds and explained previously by possible molecular reorientations (*Figure 8*; Daycock *et al*., 1968; Kawada *et al.*, 1970).

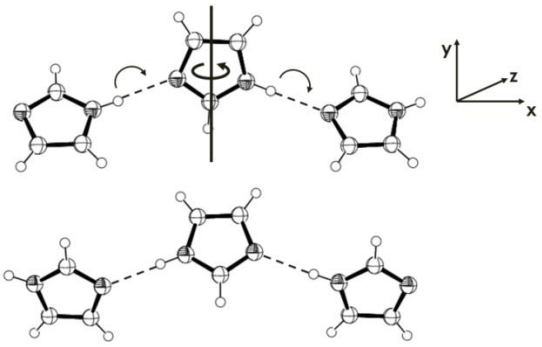

Figure 8*. Molecular reorientation model protonic conductivity in imidazole in the molten state (after Daycock et al., 1968).*

It was established that the activation energy of reorientations measured by ^1H DQ and ^{15}N NMR spectroscopies is much lower in amorphous grains than in the

crystalline state (Hickman *et al*., 1999; Fischbach *et al.,* 2004). Furthermore, in the solid state, imidazole forms centrosymmetric and non-polar crystals, which means that it does not meet the symmetry requirements of ferroelectrics materials. Only pressure-induced recrystallization of imidazole leads to its new polar phase, where the crystal acquires spontaneous polarization.

4.2 Compressibility of imidazole

Compression of imidazole is monotonic and do not reveal any anomalies. In this work, two experimental procedures were used to investigate imidazole compressibility and possible phase transitions.

A piston-cylinder device was used for the compressibility measurements (Baranowski & Moroz, 1982). First, the compressibility of kerosene was measured up to 1.9 GPa. The results of this measurement are listed and plotted in Appendix B. Then the 9.8 ml cylinder was filled with 8 g of imidazole and topped with kerosene to the final volume. Compressibility of imidazole was measured up to 1.72 GPa (*Figure 1 in Appendix A, Article A1*). Finally, the compressibility of imidazole was calculated for the measured kerosene compressibility and the known kerosene : imidazole ratio (v/v:3.5/6.5).

In the second approach, a single KUMA KM4 diffractometer was used for high-pressure single-crystal diffraction experiments.

4.3. High-pressure crystallization

0.5g of imidazole (from Polskie Odczynniki Chemiczne S.A. without further purification) was dissolved in 1ml of pure methanol, yielding the saturated solution. Tungsten gaskets of 0.2 mm thickness and with 0.45 mm diameter hole were used. A small ruby chip for pressure calibration was placed in the DAC (Diamond-Anvil-Cell) chamber. After filling the chamber, the DAC was immediately closed. Promptly after closing the DAC, a polycrystalline mass precipitated inside the chamber. The polycrystalline sample was heated with a hot-air gun until all but one crystallites dissolved at 365 K. Then, the DAC was slowly cooled down to room temperature and a single crystal of monoclinic α-phase imidazole was obtained at 0.5 GPa. The pressure in the DAC was gradually

increased and for each pressure point X-ray data were collected up to 2.7 GPa. In the new experiment, a single crystal of imidazole was isochorically recrystallized above 1.2 GPa yielding a new orthorhombic *β*-form of imidazole. A series of X-ray measurements were performed for compressed and decompressed crystals of *β*-imidazole in the pressure range from 0.5 to 3.35 GPa. The process of crystal growth of phases *α* and *β* is illustrated in *Figures 9* and *10*.

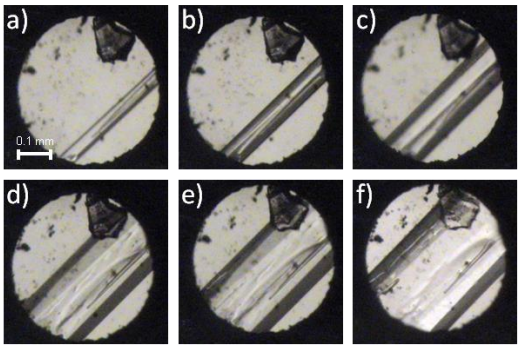

Figure 9. *Isochoric crystal growth of α-imidazole: one crystal seed at a) 370 K; b) 350 K; c) 330 K; d) 320 K; e) 310 K; and f) 296 K and 0.5 GPa before the data collection. The ruby chip for pressure calibration lies by the upper-edge of the chamber.*

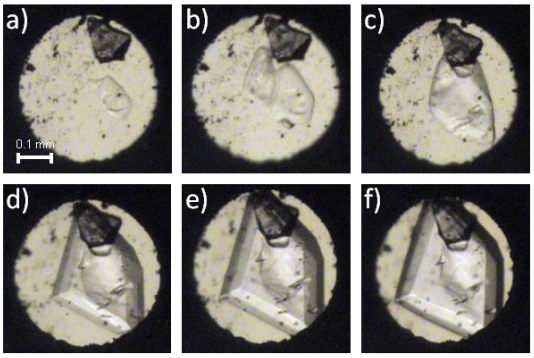

Figure 10. *The same DAC chamber as in Figure 9 and isochoric crystal growth of β-imidazole: one crystal seed at a) 450 K; b) 440 K; c) 420 K; d) 380 K; e) 330 K; and f) 296 K and 0.8 GPa before the data collection. The ruby chip for pressure calibration lies at the upper-edge of the chamber.*

4.4 Polar high-pressure structure

High pressure and temperature-induced crystallization of imidazole results in its new polar phase. It has been established, that above 1.2 GPa imidazole does not crystallize in the centrosymmetric monoclinic *α*-polymorph, but in the non-

centrosymmetric orthorhombic *β*-phase, space group *Aba*2. The polar imidazole phase is stable in the pressure range from 1.2 GPa to 3.4 GPa at least, but it can also survive the decompression to 0.2 GPa or less. The region of pressure hysteresis, where both phases can exist independently, allowed the measurements for these different phases at the same thermodynamic conditions (*Table 1 in Article A.1*).

Like in the monoclinic *α*-phase, the orthorhombic *β*-phase is built of NH···N bonded chains (*Figure 2 in Article A.1*). However, the environment of molecules in the crystal is different. The neighbouring molecules engaged in NH···N hydrogen bonds in imidazole *β* are related by translation. Furthermore, in both imidazole phases the initial lengthening of N(1)···N(3)' distances (*Figure 3 in Article A.1*), and their subsequent shortening are observed. The compression of N(1)···N(3)' distance gradually reduces the energy barrier between the two H-sites, and can facilitate the H-atom hopping. The shortest N(1)···N(3)' distance, of 2.756(8) Å evidenced in *β*-imidazole at 3.35 GPa, is by 0.093 Å shorter than in *α*-imidazole at 0.1 MPa.

In order to obtain the potential energy surface for proton transfer in the chain of hydrogen-bonded imidazole molecules arranged as in the crystal *β* phase, partially constrained geometry computational optimizations of the system were carried out using one-dimensional periodic boundary conditions. The calculations were performed with the GAUSSIAN09 program at the B3LYP/6-311G(d,p) level of theory (Gaussian 09, 2010). The translation vector $\boldsymbol{T_v} = |\mathbf{b}+\mathbf{c}|/2$ between NH···N bonded molecules located at the nodes of Bravais lattice *A* (*cf. Figure 1. in Article A.1*) was gradually shortened from 5.1 to 4.5 Å with a step of 0.01 Å, while the N(1)···H(1) distance was probed from 1.0 to 2.1 Å with a step of 0.05 Å. It was established experimentally that the length of the translation vector, with a good approximation, linearly depends on pressure (*Figure 11*). Therefore the results of potential-energy of the proton transfer path in the chain of hydrogen-bonded molecules calculated in the function of the translation T_v can be easily related to the scale of pressure. As expected, the height of energy barrier decreases with the translation vector shortening (*Figure 12*). The proton-transfer energy reaches the RT = 2.43 kJ mol^{-1} (product of the molar gas constant and the temperature at 296 K) at the translation vector length of about 4.6 Å, which corresponds to the

pressure of 12.3 GPa. This pressure is somewhat higher than that roughly estimated from linear compression of NH···N bonds. The calculations of N(1)-H(1) bond length and N(1)···N(3)' distance dependence as a function of translation vector (pressure) were aimed at comparing the compression of the isolated chain (GAUSSIAN calculations) with the chain compression in the crystal environment (experiment).

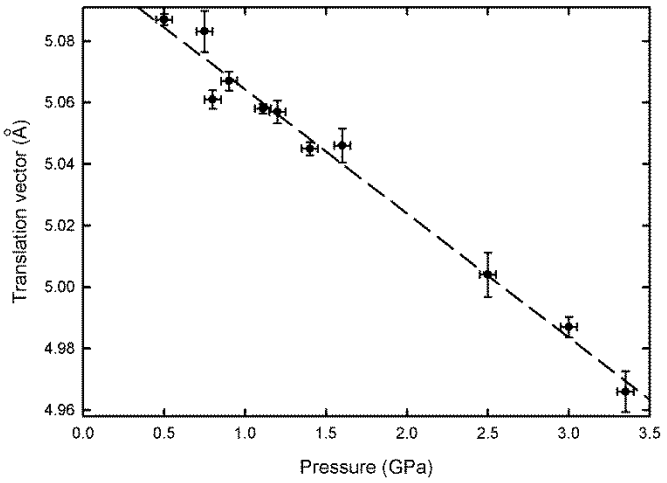

Figure 11. *The pressure dependence of translation vector (|**b**+**c**|/2 crystal translation) in the crystal structure of imidazole β phase. The experimental points are shown with bidirectional error bars. The regression line (marked by dashes) is* $T_v = -0.0411 \cdot p + 5.106$ *(Å).*

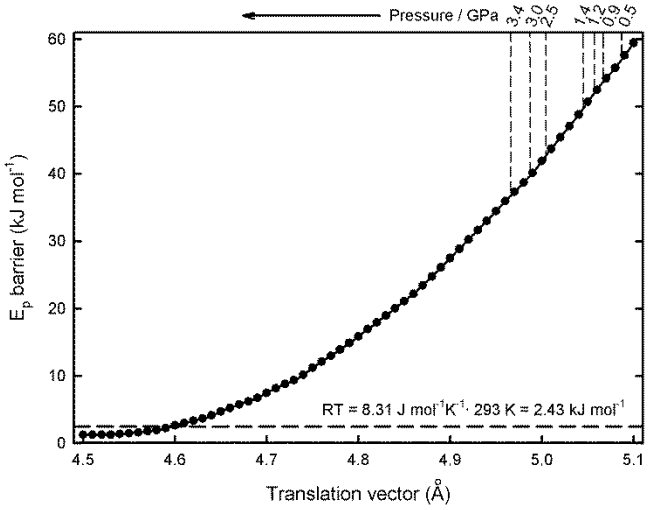

Figure 12. *Proton-transfer energy barrier* E_p *plotted in the function of translation vector* T_v *in NH···N bonded chain of imidazole molecules arranged as in the β phase. The vertical dashed lines indicate the translation vector magnitudes determined experimentally, labeled with the corresponding pressure values. The horizontal dashed line represents the RT energy threshold at room temperature.*

The calculations were performed stepwise for the chain of molecules defined as above, with the translation vector changing in the range from 5.1 to 4.5 Å. The results are presented in *Figures 13* and *14*, respectively. In *Figure 13* the experimental structural data for crystal has been added to the plot to show their agreement with the calculated values. This consistence suggests that other effects of crystal environment are minor for the compression of N···N and H···N distances.

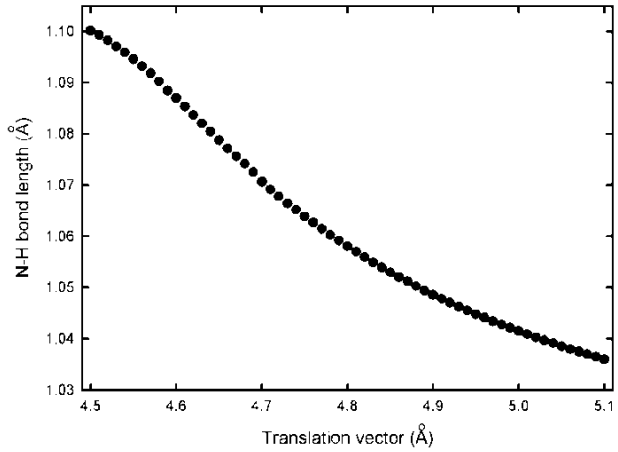

Figure 13. *The N-H bond length between NH···N bonded imidazole molecules, as a function of the chain translation vector.*

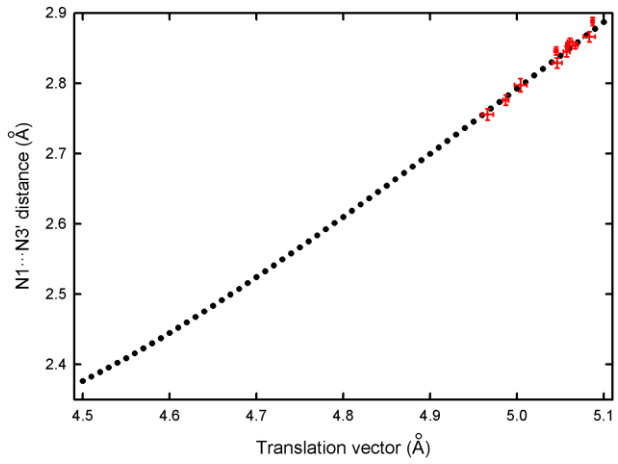

Figure 14. *The N(1)···N(3)' distance in NH···N bonded chain of imidazole molecules arranged as in the crystal β phase, in the function of translation vector. The small dots represent the experimental data, shown in red with bidirectional error bars.*

4.5 Conclusions

The pressure evolution of hydrogen bond parameters in polar β-phase agrees very well with the theoretical predictions computed for periodic imidazole chains. The calculations have also helped to model double-well energy potential in the function of pressure. Interestingly, polar β-phase of imidazole can be obtained only by high pressure recrystallization of monoclinic phase. It remains puzzling why the ambient-pressure α-phase is centrosymmetric and why high pressure is needed for obtaining the polar β-phase.

5

Pressure-induced transition in ferrocene I

Ferrocene, Fe(η^5-C_5H_5)$_2$, is the most stable example of all known till now sandwich complexes, in which metal ions are connected with cyclopentadienyl rings. Although its molecular and crystal structure was thoroughly investigated, several aspects remained unclear. For example, it was postulated that ferrocene undergoes a phase transition under high pressure at about 1.1 GPa (Duecker & Lippincott, 1967). However, in the late 1970s, the observation of this pressure transition was hampered mainly because of the technical hindrances, such as sample size and its relatively high melting point. Within this thesis a series of laboratory and synchrotron diffraction experiments were performed in order to investigate the high-pressure behavior of ferrocene.

5.1 Ambient-pressure ferrocene phases and conformations

Ambient-pressure and low-temperature structural studies of ferrocene give many significant information about the conformation and environment of ferrocene molecules in the crystal. So far, there are three well-known and structurally characterized forms of ferrocene in the literature, and also deposited in the Cambridge Structural Database. At ambient pressure and room temperature ferrocene forms monoclinic crystals of form I, space group $P2_1/a$, (Takusagawa & Koetzle, 1979). At 165 K form I transforms to triclinic form II (Seiler & Dunitz, 1982), of space group $F\bar{1}$ and the unit cell with almost doubled dimensions. Another phase was obtained at still lower temperature, when ferrocene was recrystallized at 98 K. This phase III is orthorhombic, space group *Pnma* (Seiler & Dunitz, 1979).

The energy barrier between eclipsed and staggered molecular conformation (*Figure 2*) is relatively low, of about 4 kJ/mol (Coriani *et al.*, 2006; Haaland & Nilsson, 1968). However, the molecular conformation in the ferrocene crystalline

phases is different. According to the neutron diffraction experiments, the cyclopentadienyl rings are disordered around the staggered conformation in monoclinic phase I (Takusagawa & Koetzle, 1979). By lowering the temperature rings disorder is eliminated, and after phase transition to triclinic form II, the independent molecules are ordered in somewhat distorted staggered conformations. In the structure of phase III below 98 K the molecules assume energetically favoured eclipsed conformation. The atomic displacement parameters in these conditions are very small. Table 1 summarizes crystallographic data for ferrocene phases at 98, 101 and 173 K.

Table 1. *Crystal data of ferrocene phases: monoclinic ferrocene I (Takusagawa & Koetzle, 1979), triclinic ferrocene II (Seiler & Dunitz, 1982) and orthorhombic ferrocene III (Seiler & Dunitz, 1979).*

	ferrocene I	*ferrocene II*	*ferrocene III*
crystal system	*monoclinic*	*triclinic*	*orthorhombic*
space group	$P2_1/a$	$F\bar{1}$	*Pnma*
temperature (K)	173	101	98
a (Å)	10.443	20.960	6.987
b (Å)	7.572	15.019	8.995
c (Å)	5.824	11.421	12.196
α (°)	90	89.47	90
β (°)	120.95	119.93	90
γ (°)	90	90.62	90
V (Å^3)	394.957	3115.61	766.495
Z	2	16	4
R (%)	5.3	1.9	1.9

5.2 Compression of ferrocene

A series of synchrotron and laboratory diffraction studies have been performed for ferrocene crystals up to 11.6 GPa (*Figure 1 in Article A.2*). The compression of ferrocene is unusual in this respect that one of the unit cell dimensions, parameter b, increases with increasing pressure in the pressure range between 2.0 and 4.0 GPa (the effect termed as the *U*-turn compression), and that at 3.24 GPa angle β suddenly drops across 90° (*Figure 2 in Article A.2*).

It has been established that this anomalous compression can be associated with the changes of intermolecular contacts between cyclopentadienyl rings, which leads in consequence to the pressure-induced elimination of their disorder, described in *Article A.2*.

It is amazing that above 3.24 GPa the intermolecular distances d[111] along diagonal [111] are shorter than d[-111] along diagonal [-111], and therefore the lattice strain proceed toward angle β equal 90°, when both these distances become equal above 4.0 GPa (*Figure 6 in Article A.2*). Further compression of ferrocene is monotonic and do not show any clear anomalies up to 11.6 GPa

5.3 Mechanism of pressure-induced transition

It can be postulated, basing on the *U*-turn compression of parameter *b* and subsequent ordering of the cyclopentadienyl rings conformation, that ferrocene undergoes a pressure-induced isostructural transition. This unusual phase transition results from the potential energy of intermolecular contacts interfering with the ferrocene molecular conformation. It is characteristic of isostructural phase transitions that, according to Ehrenfest, they are of the first-ordered type (Jaeger, 1998).

For the isolated ferrocene molecule the minimum of potential energy function corresponds to the eclipsed position of cyclopentadienyl rings. However, crystal environment of ferrocene molecules enforces a twisted conformation with the rings disordered. The potential function of molecular conformation has two wells (*Figure 4 in Article A.2*), consistently with the two-sites disorder model (Takusagawa & Koetzle, 1979) and with the magnitudes of atomic displacement parameters. High pressure gradually enhances the crystal-environment forces and reduces the amplitudes of thermal vibrations till 3.24 GPa, when the molecule locks in at the metastable position.

This type of phase transition, directly connected with the *U*-turn compression of crystal dimensions, for the first time proposed for ferrocene, can explain the nature of the unusual and puzzling compression of some other compounds.

5.4 Conlusions

The anomalous U-turn compression have been observed for ferrocene crystals. It has been postulated that above 3.24 GPa ferrocene I undergoes a unique phase transition to its isostructural phase I' and that this transition can be associated with the strongly anomalous compression affecting the molecular conformations.

6

Helical patterns in gold(I) diethyldithiocarbamate

Au(I) diethyldithiocarbamate polymerize into gold-gold bonded helices. At ambient conditions, these molecular filaments assume Au_8 turn intervals in tetragonal polymorph *α.* Under pressure it exhibits the negative area compressibility, due to the shortening of the length of the springs and their increased diameter. Above 0.05 GPa, the crystal transforms to the orthorhombic phase *β,* with the Au···Au wires assuming Au_{16} turn intervals. In this work, the compression of both phases and their transition were rationalized in the terms of the Au···Au bonds compression and transformation of the Au···Au bonded helices.

6.1 Aurophilic interactions

The phenomenon of aurophilicity can be defined as the tendency of the low-coordinate gold complexes to associate into dimers, oligomers, polymers and conglomerates *via* direct gold-gold contacts (Schmidbaur, 2000). However, this feature is characteristic mainly for closed-shell gold(I) compounds, with the $5d^{10}$ configuration of gold atoms. It can be assumed, that the distance between two neighbouring gold(I) centres should not exceed the sum of van der Waals radii. Generally, the average distance is 2.7-3.3Å. The energy of such interactions is relatively low, but often comparable with the energy of hydrogen bonds. (Runeberg *at al.,* 1999; Schmidbaur, 2000)

In this work, high pressure techniques have been used in order to investigate the compression of gold-gold weak interactions in gold(I) diethyldithiocarbamate polymer.

6.2 Synthesis

Sodium diethyldithiocarbamate was synthesized in the reaction of diethylamine with carbon disulphide in the presence of sodium hydroxide. 5.15 ml of diethylamine (50 mmol) in 15 ml of methanol and 2 g of sodium hydroxide (50 mmol) dissolved in 5 ml of distilled water were mixed together in a 50 ml Erlenmeyer flask. The mixture was cooled in the ice bath and stirred. Through a dropping funnel 3 ml (50 mmol) of carbon disulphide in 15 ml of methanol was carefully added to the mixture drop by drop. After 30 minutes the pale-yellow powder precipitated. The resulting precipitate was filtered off on a Büchner funnel, washed with distilled water and left to dry. Yield 67%.

Gold(I) diethyldithiocarbamate polymer $[Au_2(C_4H_{10}NCS_2)_2]_n$ was synthesized in the reaction of sodium diethyldithiocarbamate trihydrate with PPh_3AuCl gold(I) complex (from Sigma-Aldrich without further purification) in the dichloro-methane/methanol (v:v / 1:1) solution. 0.1 g of PPh_3AuCl dissolved in 2 ml of dichloromethane was added to a 2 ml of the methanol solution of sodium diethyldithiocabamate. The resulting mixture was stirred for 8 hours until colourless crystals of triphenylphosphine precipitated. The precipitate was filtered off and the solution was left for crystallization. After one day needle-like orange crystals formed in the mother-liquor.

6.3 Temperature and pressure studies

Low-temperature and high-pressure X-Ray diffraction measurements of gold(I) diethyldithiocarbamate crystals were performed using KUMA KM4 and Oxford Diffraction Xcalibur Eos diffractometers. However, high-pressure experiments were challenging in this respect that because of long unit-cell parameter *c* exceeding 45 Å the sample-detector distance had to be increased to 110 mm. It allowed optimizing the experimental conditions between x-rays absorption in air, coverage of recorded data by more distant detector and the resolution of closely located reflections. Another consequence of long lattice constants was the large number of densely distributed sample reflections of which many overlapped with the reflections from the diamond anvils. Hundreds of so overlapped reflections were scrupulously eliminated.

6.4 Corresponding phases α and β of Au_2EtDTC and its solvates

Two polymorphs of gold(I) diethyldithiocarbamate polymer, $AuEt_2DTC$, were reported: tetragonal form α, of space group $I4_1/a$, and orthorhombic form β, space group *Fddd*. I found that at ambient pressure the formation of crystals can be controlled by solvent. It has been established that the CH_2Cl_2:CH_3OH 1:1 mixture favours the formation of α-$AuEt_2DTC{\cdot}xCH_2Cl_2$, whereas of the solutions with a low contents of CH_2Cl_2, form β can be obtained. The formation of phases α and β is associated with the incorporation of CH_2Cl_2 molecules in the voids of $AuEt_2DTC$ crystals (*Figure 2 in Article A.3*). Single-crystal low-temperature and high-pressure structural studies confirmed the formation of solvated $AuEt_2DTC{\cdot}xCH_2Cl_2$, where x for different samples can assume values between ½ and 0. The guest CH_2Cl_2 molecules are strongly disordered in several orientations and their detection is hampered at room temperature because of very high atomic displacement parameters (ADP's) of CH_2Cl_2 and very strong scattering of X-rays by Au atoms (relative electron density of other atoms is low). The solvation of $AuEt_2DTC$ by CH_2Cl_2 at ambient conditions results in the significantly larger, by nearly 10 $Å^3$, molecular volume (unit-cell V/Z) of phase α larger than that of phase β.

Above 50 MPa (0.05 GPa) the tetragonal α-phase transforms to orthorhombic phase β, and that this transition is repetitively reversible, while the unsolvated orthorhombic β-phase does not transform to phase α even after long time at ambient pressure, or after hydrostatic compression. The channel-like voids in $AuEt_2DTC$ have narrowings preventing the transport of guest molecules to and out of the crystal. The CH_2Cl_2 molecules trapped in the voids are unlikely to be removed at normal conditions and reversely, high pressure do not push new guests into the voids. In principle, polymorphs should have the same composition. At ambient conditions the $AuEt_2DTC{\cdot}xCH_2Cl_2$ forms α and β indicate their different solvation (larger x in form α and lower in β). On the other hand, the solvate of α form can be transformed to form β of the same composition by high pressure.

6.5 Compressibility of $AuEt_2DTC$

High pressure study of $AuEt_2DTC$ has shown that the orthorhombic polymorph β can be compressed to 1.0 GPa without any apparent symmetry changes. Interestingly, the crystal compression can be correlated to its structure built of Au···Au bonded helices and to the collapse of channel voids. The transformation between phases α and β hardly affects the distances between the close filaments (along directions $[100]_\alpha$ and $[010]_\alpha$ in phase α). In phase α these distances slightly increase with pressure along a_α and b_α, which leads to the negative-area compression of this phase. This effect originates from the increased radius of a compressed spring. The crystal discontinuous compression on the transition to phase β mainly results of collapsed voids, becoming longer along $[010]_\beta$ and shorter along $[100]_\beta$. This indicates that the interactions between neighbouring filaments are very important for the helical modulation of filaments. Owing to the similar parallel arrangement of the filaments, phase α is a prototypic ferroelastic form and phase β is its orientational state. The mechanism of collapsing voids in phase β leads to increasingly different parameters a_β and b_β with increasing pressure (*Figure 3 in Article A.3*). The shorter parameter a_β is considerably softer than the longer b_β parameter. At still higher pressure the crystal gradually becomes more soft along $[010]_\beta$, however this direction remains the hardest in the crystal and at 1.0 GPa the difference between a_β and b_β increases to nearly 2.5 Å.

6.6 Helices of the monoatomic Au···Au filaments

Phases α and β are centrosymmetric and there are both left- and right-handed helices. The helical modulation can be connected with the intramolecular and intermolecular strain between the $AuEt_2DTC$ units. Annular S-Au-Au angles inside the $AuEt_2DTC$ monomers are between 81.4 and 95.2°. The annular torsion angles S-Au-Au-S are on average -37°, and extra-annular ones of about -63°. The compression of phase α increases the annular S-Au-Au-S angles and decreases the extra-annular ones by about 5°. The Au-Au-Au angles are of about 171° and 177°, which illustrates the directional flexibility of Au···Au bonds and their sensitivity to

the crystal environment. Despite the similar structure of phases α and β, the ligands are considerably shifted, according to the changed modulation of filaments.

This modulation change can be rationalized by increased interactions between neighbouring filaments. In phase α their helix modulation is of the opposite handiness, as illustrated in *Figure 6 in Article A.3*. The opposite handiness of helices is unfavourable for close packing, as the threads cannot efficiently fit into the grooves running in the opposite sense. The close packing can be improved when the turns at least partly reverse their handiness, as observed in the β phase (*Figure 5 in Article A.3*).

6.7 Conclusions

The monoatomic gold-gold bonded helical filaments have been observed in gold(I) diethyldithiocarbamate polymer. In the solid state, they form two different crystalline phases built of one-dimensional Au···Au bonded wires with solvent-accessible pores in between. The tetragonal α-form is built of Au···Au bonded filaments modulated into molecular Au_8-pitch helices, while in the orthorhombic β-form Au_{16}-pitch helices are observed. In this work a mixture of dichloromethane and methanol was used for gold(I) complex crystallization. In general, it can be concluded that tetragonal α-form is favoured by larger contents of CH_2Cl_2 in the solvent mixture, whereas its lower content leads to phase β. Moreover, it has been established that the formation of β phase can be also controlled by pressure and that above 50 MPa tetragonal form transforms to the orthorhombic β-form. As a consequence, gold-gold bonded helices are partly unwound by pressure.

7
Non-bonding interactions under pressure

It can be concluded that pressure is an effective tool for tuning crystal structure by changing energetical hierarchy of non-bonding forces. Pressure can induce phase transitions and structural changes, leading to new molecular arrangements, of varied physical properties, such as crystal polarity and optical properties.

Three examples of pressure-induced transformations of molecular crystals have been presented in this thesis.

High-pressure recrystallization of imidazole has led to its new polymorph, where the infinite NH···N bonded chains of molecules assume polar arrangement. The lengths of NH···N bonds are shorter in the high pressure polymorph, which facilitates proton hopping in a double-well potential. This mechanism is also supported by periodic quantum chemical calculations.

The conformation of metallocene molecules has been intensively investigated due to the very low energy barrier between staggered and eclipsed forms. It was postulated previously that at ambient conditions cyclopentadienyl rings in ferrocene are dynamically disordered in two sites. These disorder is eliminated at high pressure leading to unexpected anomalous evolution of lattice parameters with pressure.

Aurophilic interaction is a very unusual type of intermetallic bonds, in which relativistic effects play a substantial role. So far studies on the high-pressure evolution of Au···Au distances are very limited abd this work reports the first compressibility measurements of this effect. It was shown in this thesis that pressure can partly unwind helical Au···Au bonded filaments.

These three examples illustrate the fascinating variety of structural changes imposed by pressure, which in this case are unattainable in temperature studies.

8

Summary in Polish

Streszczenie w języku polskim

Ciśnienie, tak jak temperatura, jest jednym z podstawowych parametrów termodynamicznych, dzięki któremu możliwe jest kontrolowanie warunków procesów chemicznych i reakcji. Przełomem w chemii wysokich ciśnień było skonstruowanie komory z kowadłami diamentowymi, w której generowane ciśnienie może osiągnąć bardzo duże wartości. Co więcej, badania dyfrakcyjne w warunkach wysokiego ciśnienia stanowią unikatową technikę badawczą pozwalającą na poznanie oraz zrozumienie zjawisk zachodzących w warunkach ekstremalnych, takich jakie panują np. we wnętrzu Ziemi czy w kosmosie.

Celem mojej pracy doktorskiej było otrzymanie oraz charakterystyka strukturalna nowych materiałów na bazie kryształów molekularnych, w aspekcie ich przemian strukturalnych związanych z transformacjami oddziaływań między-cząsteczkowych oraz agregacją molekuł w sieci krystalicznej. W ramach doktoratu podjąłem próby otrzymania pierwszego molekularnego ferroelektryka z wiązaniami wodorowymi typu NH···N. W tym celu wybrałem kryształy imidazolu, jednego z najprostszych układów z wiązaniami typu NH···N. W warunkach atmosferycznych imidazol tworzy centrosymetryczne kryształy w układzie jednoskośnym. W wyniku ciśnieniowej rekrystalizacji w komorze z kowadłami diamentowymi otrzymałem nową, polarną odmianę polimorficzną imidazolu oraz określiłem warunki termodynamiczne, w których obie odmiany polimorficzne współistnieją. W celu wyznaczenia ściśliwości imidazolu wykonałem pomiary dyfrakcyjne z użyciem komory wysokociśnieniowej z kowadłami diamentowymi oraz prasę wysokociśnieniową typu tłok-cylinder.

Badania strukturalne kryształów ferrocenu przeprowadzone zostały w ramach współpracy z European Synchrotron Radiation Facility w Grenoble. Już na podstawie badań laboratoryjnych w kryształach ferrocenu zaobserwowałem anomalną ściśliwość jednego z parametrów strukturalnych oraz indukowane wysokim ciśnieniem wygaszenie drgań termicznych atomów węgla w pierścieniu

cyklopentadienylowym. W związku z postulowanym wcześniej modelem nieuporządkowania pierścieni cyklopentadienylowych w dwóch pozycjach, w strukturze ferrocenu w warunkach atmosferycznych, zaproponowałem model przemiany izostrukturalnej ferrocenu związanej z uporządkowaniem pierścieni w pozycji naprzemianległej.

W ramach pracy doktorskiej otrzymałem także hybrydowy nieorganiczno-organiczny materiał luminescencyjny – polimeryczny dietyloditiokarbaminan złota(I). W zależności od warunków syntezy i krystalizacji, związek ten tworzy kryształy tetragonalne lub rombowe, przy czym badania wyskociśnieniowe wskazały, że powyżej 50 MPa faza tetragonalna ulega przemianie do fazy rombowej. Wykazałem, iż przemiana fazowa dietyloditiokarbaminianu złota(I) związana jest ściśle ze zmianą ułożenia helikalnych łańcuchów złota(I) oraz ich częściowym rozwijaniem w sieci krystalicznej.

9
References

Block, S., Piermarini, G. The diamond cell stimulates high-pressure research, *Physics Today*, **1976**, *29*, 44-47.

Duecker, H. C., Lippincott, E. R., Phase transformation in ferrocene, *J. Chem. Phys*., 1967, 46, 3691-3692.

Fischbach I., Spiess H. W., Saalwaechter K., Goward G. R., Solid state NMR spectroscopic investigations of model compounds for imidazole-based proton conductors, *J. Phys. Chem. B*, **2004**, *108*, 18500-18508.

Baranowski, B., Moroz, A., Isothermic freezing pressures of organic liquids at high pressure conditions. Part II. The system benzene-thiophene within the temperature range from -30 to +100°C., *Pol. J. Chem.* **1982**, *56*, 379-391.

Besson, J. M., Pressure generation. In High-pressure Techniques in Chemistry and Physics; Holzapfel, W. B.; Isaacs, N. S., Eds.; Oxford University Press: Oxford, UK, **1997**; pp. 1-45.

Boldyreva E. V., High-pressure diffraction studies of molecular organic solids. A personal view, *Acta Crystallogr. Sect. A*, **2008**, *64***,** 218-231.

Bridgman, P. W. Change of phase under pressure. I. The phase diagram of eleven substances with especial reference to the melting curve, *Phys. Rev.* **1914**, *3*, 153-203.

Bridgman, P. W., Conant, J. B. Irreversible transformations of organic compounds under high pressures, *Proc. Nat. Acad. Sci.* **1929**, *15*, 680-683.

Budzianowski A., Katrusiak A., High-pressure crystallographic experiments with a CCD detector. In High-Pressure Crystallography; Katrusiak, A., McMillan, P. F., Eds.; Kluwer: Dordrecht, the Netherlands, **2004**, p. 157.

Bujak, M., Podsiadło, M., Katrusiak, A. 1,1-Dichloroethane: a molecular crystal structure without van der Waals contacts, *J. Phys. Chem. B*, **2008**, *112*,1184-1188.

Burt A. M., Silver A., Non-enzymatic imidazole-catalysed acyl transfer reaction and acetylcholine synthesis, *Nature New Biology* **1973**, *243*, 157-159.

Chijioke, A. D., Nellis, W. J., Soldatov, A., Silvera, I. F. The ruby pressure standard to 150 GPa, *J. Appl. Phys.* **2005**, *98*, 114905.

Coriani, S., Haaland, A., Helgaker, T., Jørgensen, P., The equilibrium structure of ferrocene, *ChemPhysChem*, **2006**, *7*, 245-249.

Daycock J. T., Jones G. P., Evans J. R. N., Thomas J. M., Rotation of imidazole in the solid state and its significance in deciding the nature of charge migration in biological materials, *Nature*, **1968**, *218*, 672-673.

Dziubek, K. F., Katrusiak, A. Compression of intermolecular interactions in CS_2 crystal, *J. Phys. Chem. B*, **2004**, *108*, 19089-19092.

Eremets, M. I., High pressure experimental methods. Oxford University Press: Oxford, UK, **1996**.

Gaussian 09, Revision B.01, M. J. Frisch, G. W. Trucks, H. B. Schlegel, G. E. Scuseria, M. A. Robb, J. R. Cheeseman, G. Scalmani, V. Barone, B. Mennucci, G. A. Petersson, H. Nakatsuji, M. Caricato, X. Li, H. P. Hratchian, A. F. Izmaylov, J. Bloino, G. Zheng, J. L. Sonnenberg, M. Hada, M. Ehara, K. Toyota, R. Fukuda, J. Hasegawa, M. Ishida, T. Nakajima, Y. Honda, O. Kitao, H. Nakai, T. Vreven, J. A. Montgomery, J. E. Peralta Jr., F. Ogliaro, M. Bearpark, J. J. Heyd, E. Brothers, K. N. Kudin,. V. N. Staroverov, T. Keith, R. Kobayashi, J. Normand, K. Raghavachari, A. Rendell, J. C. Burant, S. S.

Iyengar, J. Tomasi, Cossi M., Rega N., Millam J. M., Klene M., Knox J. E., Cross J. B., V. Bakken, C. Adamo, J. Jaramillo, R. Gomperts, R. E. Stratmann , O. Yazyev, A. J. Austin, R. Cammi, C. Pomelli, J. W. Ochterski, R. L. Martin, K. Morokuma, V. G. Zakrzewski, G. A. Voth, P. Salvador, J. J. Dannenberg, S. Dapprich, A. D. Daniels, O. Farkas, J. B. Foresman, J. V. Ortiz, J. Cioslowski, D. J. Fox, Gaussian, Inc., Wallingford CT, **2010**.

Haaland, A., Nilsson, J. E., The determination of the barriers to internal rotations by means of electron diffraction. Ferrocene and ruthenocene, *Acta Chem. Scand.,* **1968**, *22*, 2653-2670.

Hanfland, M., Syassen, K., Christensen, N. E., Novikov, D. L., New high-pressure phases of lithium, *Nature*, **2000**, *408*, 174-178.

Hazen, R.M., Finger, L.W., Comparative Crystal Chemistry. John Wiley and Sons, New York, **1982**.

Hickman B. S., Mascal M., Titman J. J., Wood I. G., Protonic conduction in imidazole: a solid-state ^{15}N NMR study, *J. Am. Chem. Soc.* **1999**, *121*, 11486-11490.

Horiuchi S., Tokunaga Y., Giovannetti G., Picozzi S., Itoh H., Shimano R., Kumai R., Tokura Y., Above-room-temperature ferroelectricity in a single-component molecular crystal, *Nature*, **2010**, *463*, 789-792.

Horiuchi, S., Kagawa, F., Hatahara, K., Kobayashi, K., Kumai, R., Murakami, Y., Tokura, Y., Above-room temperature ferroelectricity and antiferroelectricity in benzimidazoles, *Nature Commun.,* **2012**, *3*, 1308.

Jaeger, G., The Ehrenfest classification of phase transitions: introduction and evolution. *Arch. Hist. Exact Sci.* **1998**, *53*, 51-81.

Jayaraman, A., Diamond anvil cell and high-pressure physical investigations, *Rev. Mod. Phys.* **1983**, *55*, 65-108.

Katrusiak A., REDSHABS: A program for correcting reflections intensities for DAC absorption and gasket shadowing; Adam Mickiewicz University, Poznań, Poland, **2003**.

Katrusiak, A., High pressure crystallography, *Acta Crystallogr. Sect. A*, **2008**, *64*, 135-148.

Katrusiak, A., Podsiadło, M., Budzianowski, A. Association CH···π and no van der Waals contacts at the lowest limits of crystalline benzene I and II stability regions, *Cryst. Growth Des.,* **2010**, *10*, 3461-3465.

Kawada A., McGhie A. R., Labes M. M., Protonic conductivity in imidazole single crystal, *J. Chem. Phys.*, **1970**, *52*, 3121-3125.

Laidler, K. L., A glossary at terms used in chemical kinetics, including reaction dynamics, *Pure&Appl. Chem.,* **1996**, *68*, 149-192.

Lundegaard, L. F., Weck, G., McMahon, M. I., Desgreniers, S., Loubeyre, P. Observation of an O_8 molecular lattice in the epsilon phase of solid oxygen, *Nature*, **2006**, *443*, 201-204.

Ma, Y., Eremets, M., Oganov, A. R., Xie, Y., Trojan, I., Medvedev, S., Lyakhov, A. O., Valle, M., Prakapenka, V., Transparent dense sodium, *Nature*, **2009**, *458*, 182-185.

Mao, H. K., Xu, J., Bell, P. M. Calibration of the ruby pressure gauge to 800 kbar under quasi-hydrostatic conditions, *J Geophys Res: Solid Earth*, **1986**, *91*, 4673-4676.

Merrill L., Bassett, W. A., Miniature diamond anvil pressure cell for single crystal X-ray diffraction studies. *Rev. Sci. Instrum.,* **1974**, *45*, 290-294.

Miletich, R., Allan, D. R., Kuhs, W. F., High-pressure single-crystal techniques. *Rev. Mineral. Geochem.,* **2000**, *41*, 445-519.

Nazario I., Gonzalo J. A., Ferroelectric behavior of KH_2PO_4 in the critical region, *Solid State Commun.* **1969**, *7*, 1305-1308.

Ogborn, J. M., Collings, I. E., Moggach, S. A., Thompson,. A L., Goodwin, A. L., Supramolecular mechanics in a metal-organic framework, *Chem. Sci.*, **2012**, *10*, 3011-3017.

Olejniczak A., Katrusiak A., Szafrański M., Ten polymorphs of $NH^{+}\cdots N$ hydrogen bonded 1,4-diazabicyclo[2.2.2]octane complexes: supramolecular origin of giant anisotropic dielectric response in polymorph V, *Cryst. Growth. Des.*, **2010**, *10*, 3537-4546.

Pasternak, M., Farrell, J. N., Taylor, R. D., Metallization and structural transformation of iodine under pressure: A microscopic view, *Phys. Rev. Lett.* **1987**, *58*,575-578.

Piermarini, G. J., Block, S., Barnett, J. D., Forman, R. A. Calibration of the pressure dependence of the R1 ruby fluorescence line to 195 kbar. *J. Appl. Phys.* **1975**, 46, 2774-2780.

Rimmelin, J., Jenner, G., Etude des reactions pericycliques sous pression-III: Dimerisation thermique de l'isoprene par reaction de Diels-Alder, *Tetrahedron*, **1974**, *30*, 3081-3085.

Röntgen, W. C., Kurze Mittheilung von Versuchen ber den Einfluss des Druckes auf einige physykalische Erscheinungen, *Ann. Phys.,* **1892**, *45*, 98-107.

Runeberg, N., Schütz, M., Werner H. -J., The aurophilic attraction as interpreted by local correlation methods". *J. Chem. Phys.* 1999, **110**, 7210–7215.

Schmidbaur, H., The aurophilicity phenomenon: A decade of experimental findings, theoretical concepts and emerging applications, *Gold Bull.,* **2000**, *33*, 3-10.

Scott, J. F., Ferroelectric Memories, Springer-Verlag, Heidelberg, **2000**.

Seiler, P., Dunitz, J. D., The Structure of Triclinic Ferrocene at 101, 123 and 148 K., *Acta Crystallogr. Sect. B,* **1979**, *35*, 2020-2032.

Seiler, P., Dunitz, J. D., Low-temperature crystallization of orthorhombic ferrocene: structure analysis at 98 K., *Acta Crystallogr. B,* **1982**, *38*, 1741-1745.

Sheldrick, G. M. A short history of SHELX, *Acta Crystallogr. Sect. A* **2008**, *64*, 112-122.

Sikora, M., Katrusiak, A., Pressure-controlled neutral-ionic transition and disordering of NH···N hydrogen bonds in pyrazole, *J. Phys. Chem. C*, **2013**, *117*, 10661-10668.

Syassen, K., Ruby under pressure, *High Pressure Research*, **2008**, *28*, 75-126.

Szafrański, M., Katrusiak, A., Short-range ferroelectric order induced by proton transfer-mediated ionicity, *J. Phys. Chem. B*, **2004**, *108***,** 15709–15713.

Szafrański M., Katrusiak A., McIntyre G. J., Proton disorder in NH···N bonded [dabcoH]$^{+}$I^{-} relaxor: New insights into H-disordering in a one dimensional H_2O ice analogue, *Cryst Growth. Des.,* **2010**, *10*, 4334-4338.

Takusagawa, F., Koetzle, T. F., A Neutron diffraction study of the crystal structure of ferrocene. *Acta Crystallogr. Sect. B,* **1979**, *35*, 1074-1081.

Van Eldik, R., Hubbard, C. D., in: High pressure chemistry - synthetic, mechanistic, and supercritical applications, Van Eldik, R., Klärner, F.-G., Eds. Wiley-VCH: Weinheim, **2002**, pp. 6-12.

Weir, C. E., Lippincott, E. R., Van Valkenburg, A., Bunting, E. N., Infrared studies in the 1- to 15-micron region to 30,000 atmospheres, *J. Res, Natl. Bur. Stand.,* **1959**, *63A*, 55-62.

Werner, H., At least 60-years of ferrocene: the discovery and rediscovery of the sandwich complexes*, Angew. Chem. Int. Ed*., 2012, *51*, 6052-6058.

Yoshizawa M., Ogihara W., Ohno H., Design of new ionic liquids by neutralization of imidazole derivatives with imide-type acids, *Electrochem. Solid-State Lett.,* **2001**, *4*, E25-E27.

Zhang, W., Oganov A. R., Goncharov, A. F., Zhu, Q, Boulfelfel S. E., Lyakhov, A. O., Stavrou, E., Somayazulu, M., Prakapenka, V. B., Konôpková Z., Unexpected stable stoichiometries of sodium chlorides, *Science* , **2013**, *342*, 1502-1505.

10
Appendix A: Scientific articles

Article A.1

D. Paliwoda, K. Dziubek, A. Katrusiak,

Imidazole hidden polar phase,

Cryst. Growth Des. 2012, *12*, 4302-4305.

CRYSTAL GROWTH & DESIGN

Communication

pubs.acs.org/crystal

Imidazole Hidden Polar Phase

Damian Paliwoda, Kamil F. Dziubek, and Andrzej Katrusiak*

Department of Materials Chemistry Faculty of Chemistry, Adam Mickiewicz University, Grunwaldzka 6, 60-780 Poznań, Poland

Supporting Information

ABSTRACT: Transformations of NH···N hydrogen bonds can be employed in new classes of electronic materials. Imidazole, a prototypic NH···N bonded crystal, remains centrosymmetric when compressed to 2.7 GPa. However, its recrystallization at 1.2 GPa leads to a new polar phase which in turn can be decompressed to 0.5 GPa at least. This transformation and calculated potential-energy function of the H-atom correlate with the transforming dimensions of the hydrogen bond and reveal high polarity of nonionic NH···N bonded compounds.

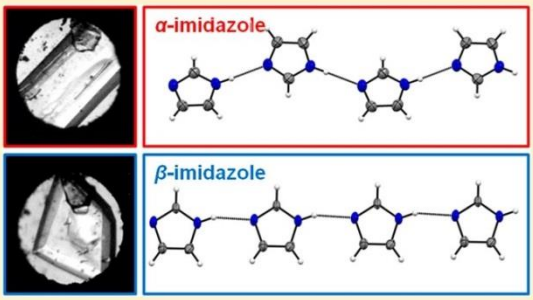

One of the simplest NH···N bonded compounds is imidazole, $C_3H_4N_2$, a diazine of particular biochemical[1] and chemical importance.[2] Owing to the predictable pattern of hydrogen bonds linking the molecules into chains, imidazole is a model compound for the NH···N bonded structures and for the proton transfer, after the electron transfer the most frequent phenomenon in Nature. Imidazole also exhibits ionic conductivity, which has been associated with the proton transfer in NH···N bonds and previously explained by molecular reorientations.[3] It was found by ^{1}H DQ and ^{15}N NMR spectroscopies that the activation energy of reorientations is much lower in amorphous grains than in the crystalline state,[4] which suggests that the structures with long NH···N bonds can reverse polarity easily in micro- and nanosized grains. This pertains to ferroelectric and relaxor properties, when electric permittivity amounts to giant magnitudes exceeding 1000. Most presently used materials of this kind are perovskite ceramics doped with lead.[5] In principle, organic substances could afford cheaper, greener, more efficient, and smaller electronic devices. Most recently, ferroelectric properties were found in OH···O bonded croconic acid[6] analogous to those in KH_2PO_4 (KDP).[7] Also new functional materials with bistable NH^+···N bonds acting as microswitches of domain polarity, have been reported.[8] Monosalts of 1,4-diazabicyclo[2.2.2]octane (dabco) of general formula dabcoHX when X^- is the tetrahedral anion ClO_4^-, BF_4^-, or ReO_4^- are ferroelectrics and those with anions X^- = Br^- or I^- are stoichiometric anisotropic relaxors.[9] However, until now, no nonionic molecular NH···N bonded ferroelectrics have been found.

The nonionic forms of NH···N hydrogen-bonded imidazoline derivatives have been considered as promising materials for optoelectronic materials.[10] In order to efficiently design the structures of such materials, it is essential to understand the transformations of NH···N bonds and the factors destabilizing the protons. It was established that NH···N bonds are highly polarizable, and their transformations were extensively studied by spectroscopic[11] and structural methods.[12] Moreover, the effect of pressure, strongly affecting the KDP ferroelectrics,[13] has been hardly studied for NH···N bonded materials. Here we show that imidazole, a prototypic compound in chemistry and biology, can be transformed into a polar phase (β) and that the proton site in NH···N bonds strongly depends on the molecular arrangement and crystal-structure environment. In light of our study, the NH···N bonded molecular compounds are promising alternatives of presently used ferroelectrics and relaxors. An exceptionally large metastable region revealed in this study on imidazole shows that also other compounds may require in situ crystallizations for transforming to new polymorphs.

At ambient pressure, no polymorphic transformations of the monoclinic imidazole, space group $P2_1/c$,[14] hereinafter denoted as phase α, have been observed between 103 K and the melting point at 364 K. Recrystallization of imidazole at high pressure induces a new phase, where the polarity of NH···N bonds and crystal polarization become coupled. We have applied two experimental procedures, which proved crucial for revealing the high-pressure phase of imidazole. In the first approach, in order to obtain a possibly high-quality imidazole single crystal, it was grown in situ in the diamond-anvil-cell (DAC) at isochoric conditions from saturated methanol solution. Then pressure was gradually increased and several diffraction data sets were recorded for this sample up to 2.7 GPa. In all this pressure range, the sample remained in the ambient-pressure phase α. In the second approach, in situ crystallizations were probed at gradually increased pressure, and a single crystal of new

Received: June 25, 2012
Revised: July 20, 2012
Published: July 24, 2012

 © 2012 American Chemical Society dx.doi.org/10.1021/cg300852t | Cryst. Growth Des. 2012, 12, 4302−4305

imidazole polymorph β was obtained above 1.2 GPa. The sample was dissolved by heating and then slowly cooled to allow nucleation and crystal growth. The crystal habits of phases α and β are easily distinguishable (Figure 1).

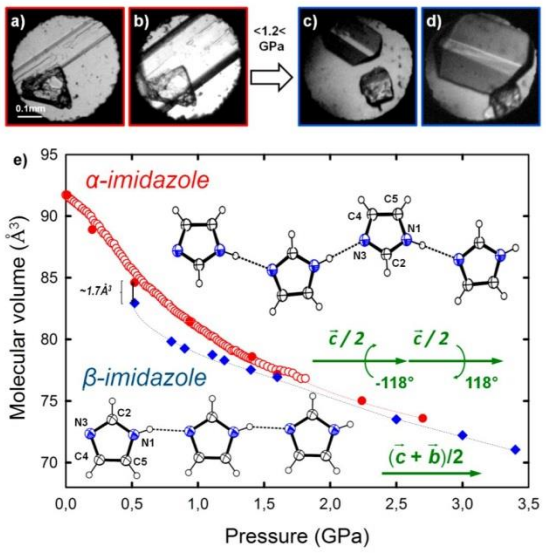

Figure 1. Isochoric in situ crystal growth of imidazole dissolved in methanol, in a diamond-anvil cell: (a) a single crystal of phase α at 390 K; (b) at 296 K and 0.5 GPa; (c) a crystal of β-imidazole at 450 K; and (d) at 296 K and 1.2 GPa; cell contains the ruby chip for pressure calibration; (e) the pressure dependence of molecular volume of imidazole crystals measured in a piston-cylinder device up to 1.72 GPa (red open circles) and by X-ray diffraction for imidazole phases α (full red circles) and β (blue diamonds). The insets show H-bonded chains in phases α (top) and β (bottom). The translations and rotations between neighboring molecules are shown by green arrows.

The compressibilities of phases α and β are different (Figure 1), but their molecular volumes become very similar above 2.5 GPa. This explains the unexpectedly large range of pressure, between 1.2 and 2.7 GPa, where the molecular-volume difference and, hence, the work component of the Gibbs free energy, is small. The single crystal of imidazole β survived decompression below 1.2 GPa. Its diffraction data could be measured down to 0.5 GPa only; however, it was observed optically at still lower pressure. The crystal gradually dissolved and finally shuttered at 0.2 GPa. The X-ray powder diffraction pattern of the shuttered sample recovered from the DAC was consistent with the α-phase. All other attempts to recover the β-phase crystal from the DAC failed.

It has been established, based on repeated in situ crystallizations, that phase α is stable between 0.1 MPa and 1.2 GPa, and phase β is stable above 1.2 GPa. Both phases exhibit an anormous hysteresis: phase α can remain in the metastable state at least 1.5 GPa (from 1.2 to 2.7 GPa) over the stability region of the phase β, and phase β remains metastable on decompression from 1.2 to 0.2 GPa at least. This allowed the crystal data of both polymorphs α and β to be determined under the same thermodynamic conditions (Table 1).

It is remarkable that in situ crystallizations were necessary for revealing the β-polymorph; otherwise, its existence would be masked by the large metastable range of phase α (Figure 1), as

Table 1. Crystal Data of Imidazole α and β at 0.5 GPa

space group	$P2_1/c$ (α-phase)	$Aba2$ (β-phase)
a (Å)	7.577(3)	14.250(8)
b (Å)	5.282(3)	8.623(4)
c (Å)	9.727(5)	5.399(4)
β (deg)	119.64(4)	90
V (Å^3)	338.4(3)	663.5(6)
Z	4	8
D_x (g·cm^{-3})	1.336	1.363
wR (all data)	0.0995	0.0858

evidenced to 2.7 GPa by the compressibility measurement in a piston-cylinder press to 1.72 GPa and X-ray diffraction measurements. By growing single crystals of β-imidazole, we were able to collect its X-ray diffraction data in the laboratory and to solve its structure. It is orthorhombic, space group $Aba2$ (Table 1).

The structure of phase β is built of NH···N bonded chains (Figure 2), similarly as phase α. However, the crystal of

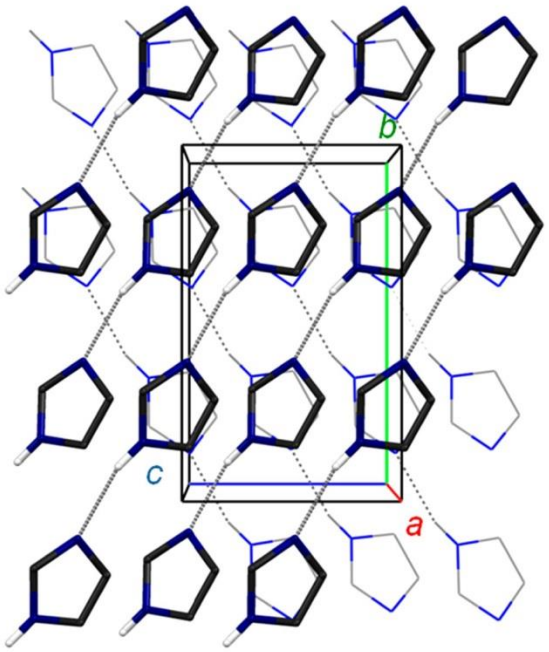

Figure 2. Arrangement of H-bonded imidazole molecules in the high-pressure β-polymorph, viewed as an autostereogram down [100].

α-imidazole is centrosymmetric, whereas that of β-imidazole is polar along [z]. Thus, the charge distribution of all atoms along [z] contributes to the polarity of the crystal. The charge distribution along the H-bonds is dominant. Polarization p_s of the β-imidazole crystal at 0.9 GPa, calculated by the PIXEL method,[15] is 8.12 μC·cm^{-2} and is nearly fully reversed, to the magnitude p_s = −7.93 μC·cm^{-2}, for the hypothetical structure where atom H(1) is shifted to the opposite site of the hydrogen bond at atom N(3)′.

The crystal total lattice energy, E_{latt}, calculated by PIXEL for the β-phase, is −86.6 kJ·mol^{-1}, compared to the higher E_{latt} = −84.2 kJ·mol^{-1} of the hypothetical structure with atoms H(1) moved to N(3)′ (Table 2). This energy difference, ΔE = 2.4

dx.doi.org/10.1021/cg300852t | Cryst. Growth Des. 2012, 12, 4302−4305

Table 2. Comparison of the Molecule−Molecule Interactions in the NH···N Hydrogen Bonded Pairs (HB) and Total Lattice Energies (latt) Calculated by PIXEL for α and β Phases

phase	p (GPa)	E_{HB} (kJ·mol^{-1})	E_{latt} (kJ·mol^{-1})
α	0.5	−43.8	−90.2
α	2.7	−42.3	−86.8
β	0.5	−41.8	−87.4
β	3.35	−37.5	−80.6

kJ·mol^{-1}, is twice larger per one H-bond than that in 2,4,6-trimethylbenzoic acid,[16] where protons are 61:39% disordered in OH···O bonds at 296 K. In this respect, the calculated magnitude of ΔE is consistent with the ordered protons observed in β-imidazole. The ΔE value in β-imidazole can be translated into the differences in the crystal environment of the H-donor and acceptor sites. The most immediate environments of the donor and acceptor sites are most likely to have the largest energetical effect for the H-site at one of the nitrogen atoms between NH···N bonded molecules. It was postulated that more favored is this H-site, for which the H···N distance is shorter.[17] Thus, for a given NH···N bond, a positive difference δ of distances H(1)···N(3)′ (δ_1, observed) subtracted from N(1)···H(3)′ (δ_2, hypothetical) would indicate the favored site. The δ parameters in both phases α and β indeed are positive and similar in magnitude, but they are slightly larger in phase β (see Supporting Information: Figure S4). Within the experimental uncertainty, the δ parameters are hardly pressure dependent, in all the pressure range investigated, which suggests that the H-atom position is stabilized by the molecular orientation in a compressed crystal environment.

The effect of pressure in both imidazole phases is the initial lengthening of the N(1)···N(3)′ distances (Figure 3), and their

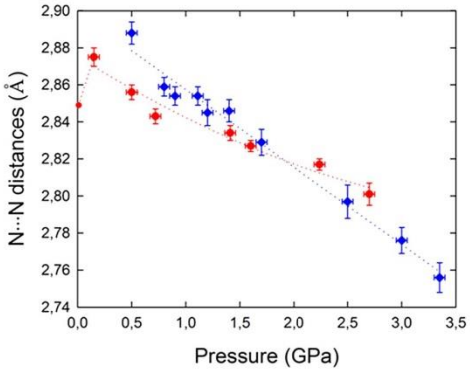

Figure 3. Pressure dependence of the N(1)···N(3)′ distance between two H-bonded imidazole molecules in α (red circles) and β (blue diamonds) polymorphs.

subsequent shortening. The compression of the N(1)···N(3)′ distance gradually reduces the energy barrier between the two H-sites and can facilitate the H-atom hopping. The most compressed N(1)···N(3)′ distance, of 2.756(8) Å, evidenced in β-imidazole at 3.35 GPa, is 0.093 Å shorter than that in α-imidazole at 0.1 MPa. This compression of about 4.2 × 10^{-2} Å·GPa^{-1} would require about 8 GPa for reducing the N(1)···N(3)′ distance to 2.554 Å, corresponding to that in the cation of proton sponge 1,8-bis(dimethylamino)-naphthalene (DMANH$^+$), where the proton assumes the central position.[18] However, intrinsic nonlinear compression would shift this estimated pressure to considerably higher values. The pressure magnitude required for lowering the potential energy (E_p) barrier to the RT (R is the gas constant and T is temperature) value at room temperature is 12.3 GPa, according to the one-dimensional periodic boundary condition calculations at the B3LYP/6-311G(d,p) level of theory (Figure 4, Supporting Information: Figures S6, S7, S8). The barrier

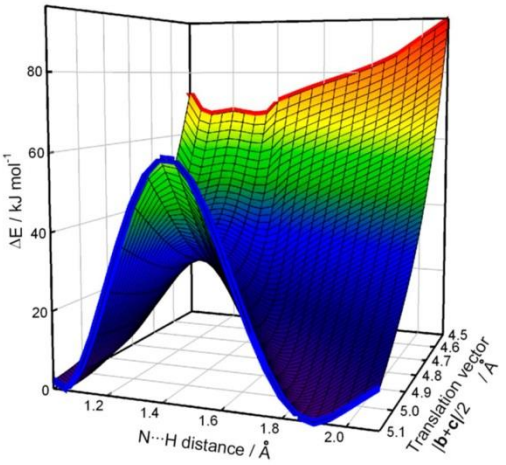

Figure 4. Potential energy surface for the proton transfer in a one-dimensional chain of NH···N hydrogen bonded imidazole molecules in the structure of phase β in the function of translation vector T_v between the H-bonded molecules, calculated theoretically (cf. Supplementar Information).

height, calculated for the β-phase at ambient pressure (for estimated NH···N dimensions at 0.1 MPa) is considerably lower than that for phase α.[19]

The phase transition between imidazole phases α and β is accompanied by a volume collapse of about 1.70(4) Å^3 per molecule (at 0.5 GPa) and a reconstruction of the NH···N bonded chains (Figure 1). In phase α the molecules in the chain are inclined by 118°, but the NH···N bond is nearly linear and it is directed approximately along the bisectors of angles C−N−C. This testifies that the NH···N bonds in phase α are hardly strained by other interactions in the crystal environment.

In high-pressure phase β, the hydrogen bonds are strongly strained and bent to an N−H···N angle of about 157°. This reflects the enhanced influence of van der Waals contacts and the diminishing role of the H-bonds. It is plausible that this reduced role of H-bonds results in the N···N distance lengthening at 0.5 GPa in phase α and in the 0.5−0.9 GPa range in phase β (Figure 3). The parallel position of molecules in phase β minimizes the H(5)···H(4)′ distances to 2.570 Å at 3.35 GPa and reduces the size of intermolecular voids. This arrangement of molecules in phase β is more compact than that in phase α, where the rings of NH···N bonded molecules are inclined and the H(5)···H(4)′ distances are much longer. This more compact arrangement is gained at the cost of strained H-bonds in phase β.

The transition between imidazole phases α and β strongly resembles the phase transition between benzene phases I and II at 1.3 GPa.[20] It was described as a sluggish transition, because it

dx.doi.org/10.1021/cg300852t | Cryst. Growth Des. 2012, 12, 4302−4305

required 3.0 GPa at 293 K, before benzene I transformed to benzene II in a sluggish way.[21] When heated above 400 K, the transition to benzene II proceeded more sharply at 1.2 GPa. Likewise, the imidazole α compressed to 2.7 GPa at 296 K does not transform at all, and in situ crystallizations were necessary for obtaining the β-phase. It is very likely that many other substances possess hidden phases that cannot be revealed by isothermal compression. This would also mean that the number of polymorphs presently revealed by compressing ambient-pressure phases[22] can be considerably increased by performing high pressure in situ crystallizations.[23]

■ ASSOCIATED CONTENT

Supporting Information

Experimental section, crystal growth, crystal data, and structural details for all measurements of imidazole phases α and β; the compressibility of imidazole α and β; and PIXEL and periodic DFT calculations. This material is available free of charge via the Internet at http://pubs.acs.org.

■ AUTHOR INFORMATION

Corresponding Author

*E-mail: katran@amu.edu.pl.

Notes

The authors declare no competing financial interest.

■ ACKNOWLEDGMENTS

This study was supported by the TEAM 2009-4/6 grant of the Foundation for Polish Science. Proton transfer calculations were performed at the Poznań Supercomputing and Networking Center.

■ REFERENCES

(1) Burt, A. M.; Silver, A. *Nature New Biol.* **1973**, *243*, 157.

(2) Yoshizawa, M.; Ogihara, W.; Ohno, H. *Electrochem. Solid-State Lett.* **2001**, *4*, E25.

(3) (a) Daycock, J. T.; Jones, G. P.; Evans, J. R. N.; Thomas, J. M. *Nature* **1968**, *218*, 672. (b) Kawada, A.; McGhie, A. R.; Labes, M. M. *J. Chem. Phys.* **1970**, *52*, 3121. (c) McDermott, L. W.. *J. Magn. Reson.* **2012**, DOI: http://dx.doi.org/10.1016/j.mr.2012.05.019.

(4) (a) Hickman, B. S.; Mascal, M.; Titman, J. J.; Wood, I. G. *J. Am. Chem. Soc.* **1999**, *121*, 11486. (b) Fischbach, I.; Spiess, H. W.; Saalwächter, K.; Goward, G. R. *J. Phys. Chem. B* **2004**, *108*, 18500.

(5) Blinc, R. *Advanced Ferroelectricity*; Oxford University Press: New York, 2011.

(6) (a) Horiuchi, S.; Tokunaga, Y.; Giovannetti, G.; Picozzi, S.; Itoh, H.; Shimano, R.; Kumai, R.; Tokura, Y. *Nature* **2010**, *463*, 789. (b) Horiuchi, S.; Tokura, Y. *Nat. Mater.* **2008**, *7*, 357.

(7) Nazario, I.; Gonzalo, J. A. *Solid State Commun.* **1969**, *7*, 1305.

(8) Olejniczak, A.; Katrusiak, A.; Szafrański, M. *Cryst. Growth. Des.* **2010**, *10*, 3537.

(9) Szafrański, M.; Katrusiak, A.; McIntyre, G. J. *Cryst Growth. Des.* **2010**, *10*, 4334.

(10) Morimoto, M.; Irie, M. *Chem. Commun.* **2011**, *47*, 4186.

(11) (a) Rabold, A.; Bauer, R.; Zundel, G. *J. Phys. Chem.* **1995**, *99*, 1889. (b) Zundel, G. *Adv. Chem. Phys.* **2000**, *111*, 1.

(12) (a) Baldy, A.; Elguero, J.; Faure, R.; Pierrot, M.; Vincent, E. −J. *J. Am. Chem. Soc.* **1985**, *107*, 5290. (b) Smith, J. A. S.; Wehrle, B.; Aguilar-Parilla, F.; Limbach, H. −H.; Foces-Foces, M.; Cano, F. H.; Elguero, J.; Baldy, A.; Pierrot, M.; Khurshid, M. M. T.; Larcombe-McDouall, J. B. *J. Am. Chem. Soc.* **1989**, *111*, 7304.

(13) Samara, G. A. *Phys. Rev. Lett.* **1971**, *27*, 103.

(14) (a) Martinez-Carrera, S. *Acta Crystallogr.* **1966**, *20*, 783. (b) Craven, B. M.; McMullan, R. K.; Bell, J. D.; Freeman, H. C. *Acta Crystallogr., B* **1977**, *33*, 2585. (c) McMullan, R. K.; Epstein, J.; Ruble, J. R.; Craven, B. M. *Acta Crystallogr., B* **1979**, *35*, 688.

(15) Gavezzotti, A. *New J. Chem.* **2011**, *35*, 1360.

(16) Wilson, C. C.; Goeta, A. E. *Angew. Chem., Int. Ed.* **2004**, *43*, 2095.

(17) Katrusiak, A. *J. Mol. Struct.* **1999**, *474*, 125.

(18) Pyżalska, D.; Pyżalski, R.; Borowiak, T. *J. Cryst. Spectrosc. Res.* **1983**, *13*, 211.

(19) Chojnacki, H. *J. Mol. Model.* **2007**, *13*, 809.

(20) Katrusiak, A.; Podsiadło, M.; Budzianowski, A. *Cryst. Growth Des.* **2010**, *10*, 3461−3465.

(21) Posiadło, M.; Jakóbek, K.; Katrusiak, A. *CrystEngComm* **2010**, *12*, 2561.

(22) Patyk, E.; Skumiel, J.; Podsiadło, M.; Katrusiak, A. *Angew. Chem., Int. Ed.* **2012**, *51*, 2146.

(23) (a) Boldyreva, E. V. *Acta Crystallogr., A* **2008**, *64*, 218. (b) Boldyreva, E., Dera, P., Eds. *High-Pressure Crystallography: From Fundamental Phenomena to Technological Applications*; Springer: Dordrecht, 2010.

Article A.2

D. Paliwoda, K. Kowalska, M. Hanfland, A. Katrusiak,

U-Turn compression to a new isostructural ferrocene phase,

J. Phys. Chem. Lett. 2013, *9*, 4034-4039.

THE JOURNAL OF PHYSICAL CHEMISTRY Letters

Letter

pubs.acs.org/JPCL

U-Turn Compression to a New Isostructural Ferrocene Phase

Damian Paliwoda,[†] Katarzyna Kowalska,[†] Michael Hanfland,[‡] and Andrzej Katrusiak*[,†]

[†]Faculty of Chemistry, Adam Mickiewicz University, Umultowska 89b, 61-614 Poznań, Poland

[‡]European Synchrotron Radiation Facility, B.P. 220, 38043 Grenoble, France

Supporting Information

ABSTRACT: Ferrocene exhibits a most intriguing transformation reflected in highly anomalous compression of the crystal, involving a discontinuity in unit-cell parameter c and reversed sign of compression coefficient $\beta_b = 1/b \cdot \partial b/\partial p$. The origin of this unexpected property is connected to the rotational and vibrational states of bis(cyclopentadienyl)iron(II) molecules in the crystal environment transformed under the high-pressure conditions. At ambient pressure, the cyclopentadienyl rings are conformationally disordered in the double-well potential energy E_p function in the structure of ferrocene phase I. Above 3.24 GPa, the single-well E_p function prevails due to intermolecular interactions enhanced by pressure, which leads to the unprecedented isostructural phase transition to the ordered ferrocene phase I′. Combined laboratory and synchrotron diffraction as well as Raman spectroscopy have been applied for describing structural transformations associated with this unique phase transition.

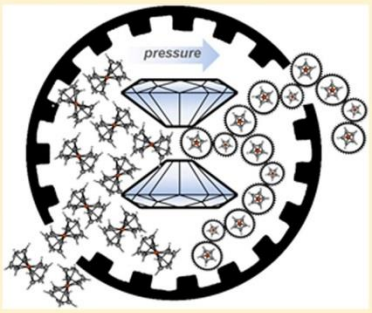

SECTION: Molecular Structure, Quantum Chemistry, and General Theory

The serendipitous discovery and first synthesis of ferrocene over six decades ago[1,2] ignited organometallic chemistry, which quickly became one of main branches of chemical sciences.[3,4] Since then, thousands of metallocenes have been synthesized and their catalytic and biological activity characterized.[5] The prototypic structure of ferrocene, although extensively investigated, has remained enigmatic in several aspects of the molecular and crystal structure as well as in its properties. In the crystal structure at room temperature, denoted as ferrocene I, of monoclinic space group $P2_1/n$, the Fe^{2+} cation is located at the inversion center and sandwiched between parallel staggered cyclopentadienyl (Cp) rings. It was found later that this ferrocene I structure is also common for other prototypic metallocenes, for example, $NiCp_2$,[6] VCp_2,[7] and $MgCp_2$.[8] Later, several other models of the $FeCp_2$ structure, involving multiple disorder of the Cp rings, were based on repeated X-ray[9] and neutron diffraction studies.[10] Here we have resolved the controversial structural models of ferrocene, and we show that its exceptional features result in the most unusual strongly anomalous compression along [010]: db/dp is initially negative, positive between 2.0 and 4.0 GPa, and then negative again. This unique property results in the interplay of molecular dynamics and the balance of conformational energy with specific intermolecular interactions. Laboratory and synchrotron single-crystal X-ray diffraction and Raman spectroscopy have been applied for precise lattice and structural determinations up to 11.6 GPa and for explaining the occurrence of metastable staggered conformation of molecules in new phase I′ of ferrocene.

Ferrocene, a prototypic metallocene, $Fe(\eta^5\text{-}C_5H_5)_2$ [$FeCp_2$], was obtained by Pauson and Kealy as a byproduct of the synthesis of dihydrofulvalene.[1] The sandwich-like structure of $FeCp_2$ had been deduced from spectroscopic data before the X-ray diffraction studies were performed.[1−4] Later, low-temperature studies of ferrocene evoked doubts regarding the molecular conformation: below 164 K, ferrocene I transforms to a triclinic phase II, space group $P\bar{1}$, where two symmetry-independent molecules are located at general positions and the Cp rings divert by ∼9° from the eclipsed conformation.[11] The structure of this triclinic ferrocene phase II is closely related to the monoclinic ferrocene phase I because the main transformation concerns the molecular conformation and displacements of the positions of molecules are small. To illustrate this relation, Seiler and Dunitz[11] described the structure of ferrocene II in an unconventional space group $F\bar{1}$ and in the unit cell with parameters a, b, and c approximately doubled compared with those of phase I. In yet another orthorhombic phase III, crystallized in situ at 98 K, the rings are exactly eclipsed.[12] Thus, the orientation of the Cp rings is different in phases I, II, and III. Moreover, a new polymorphic form of ferrocene was postulated for the sample subjected to non-hydrostatic compression and recovered to ambient conditions. The observation of a new phase based on an increase in dielectric permittivity of the precompressed sample recovered to 0.1 MPa was reported,[14] but no compressibility or high-pressure structure of ferrocene have been determined.

The compression of ferrocene I to 68% of its initial volume at 11.6 GPa is monotonic and without obvious anomalies (Figure 1). The compression of unit-cell dimensions is monotonic to

Received: October 18, 2013
Accepted: November 8, 2013
Published: November 8, 2013

ACS Publications © 2013 American Chemical Society

dx.doi.org/10.1021/jz402254b | J. Phys. Chem. Lett. 2013, 4, 4032−4037

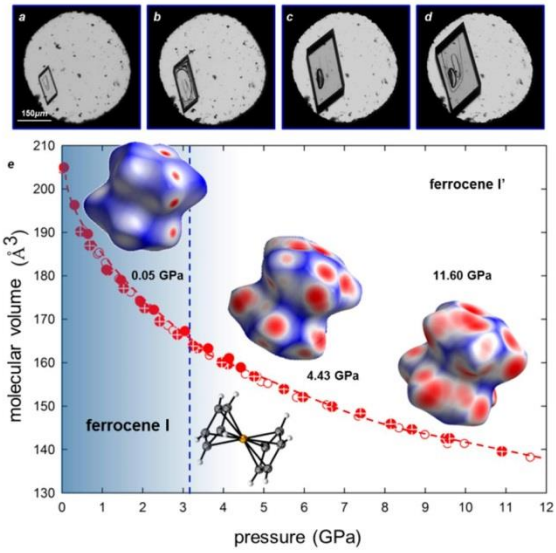

Figure 1. Isochoric in situ crystal growth at 510 K (a), 453 K (b), 363 K (c), and 296K/0.33 GPa (d) as well as the pressure dependence of molecular volume of monoclinic ferrocene phases I and I′, separated by the dashed line at 3.24 GPa. The filled circles represent laboratory data, while crossed circles and empty circles represent the compression and decompression runs measured at synchrotron, respectively. The insets show the ferrocene molecule as well as its Hirshfeld surfaces[13] decorated by color scale of intermolecular interactions (blue, longer than the van der Waals radii; white, equal to; and red, shorter) at selected pressure points.

~2.0 GPa (Figure 2), too. However, then parameter c anomalously decreases and parameter b increases. Above 2.5 GPa, parameter c decreases even faster, parameter b starts to expand ($db/dp > 0$), and angle β increases its pressure dependence, and at ~3.24 GPa it suddenly drops to 90° and a discontinuity also occurs in parameter c. It coincides with a reversal in the pressure dependence of b. At still higher pressure, between 3.24 and 4.0 GPa, angle β becomes smaller than 90°, the anomalous compression of b saturates, and then the unit-cell parameters resume monotonic contraction again. Despite the strongly anomalous compression, no symmetry change of the crystal takes place up to 11.6 GPa. Although the β angle crosses the value of 90° at ~3.24 GPa, the crystal remains monoclinic in space group $P2_1/n$. Likewise, we detected no indication of any symmetry change in the Raman spectra up to 11.9 GPa (Figure S3 in the Supporting Information).

In original determinations of ferrocene I, monoclinic space group $P2_1/a$ was applied.[9,10] However, for our study, we have chosen the monoclinic setting of space group $P2_1/n$ because the β angle of its unit cell exceeds 90° by only a few degrees. Furthermore, in this setting, angle β is reduced by pressure, and at ~3.24 GPa it abruptly assumes 90° opening, which coincides with the discontinuity in the crystal compression along [001] and with the inflection point in the compressibility along [010] (Figure 2). Above 3.24 GPa, pressure further reduces angle β, consistently with the crystal monoclinic symmetry.

The compression of ferrocene is correlated to the vibration of *Cp* rings. The rings strongly rotate at 293 K about the molecular C_{5i} axis, as illustrated in Figure 3. The strongest displacement parameters are tangential to the ring, consistent with the *Cp*-rings disorder.[10] In the two-sites model at 298 K, the disordered sites are located 0.548 Å apart, which corresponds to the rotation-angle range of 26.5° (i.e. 22.75° < τ < 49.25°, where τ measures the angular displacement of the *Cp* rings from the eclipsed conformation, as illustrated in Figure 4) about the C_5 axis and at 173 K, 0.511 Å, and 24.2°, respectively.[10] The distances between the sites of carbon atoms are so small that the disordered models could be refined only on high-resolution neutron data, where also the scattering by deuterium atoms, nearly two times further apart than the C-atoms, significantly contributed to the diffraction. Because only the carbon atoms significantly contribute to X-ray diffraction, even our high-resolution synchrotron data afforded refinements of the model, where the *Cp*-ring carbon and hydrogen atoms strongly vibrate about their single average sites, one for each atom. Such a refinement resulted in large atomic displacement parameters (ADPs) covering the C-atoms disordered in multiple sites, located along the ring circle. In this model, the *Cp* ring vibrates about the average position of the staggered conformers at τ equal to 36°; the angular amplitudes of the vibrations can be expressed as:

$$|\tau - 36°| = \cos^{-1}[(U_1 - U_3)/R] \quad (1)$$

where R is the radius from the *Cp* ring center to the trajectory of ring atoms (the radius of atomic vibrations) and U_i are the principal semiaxes of the vibrational ellipsoid (Figure 3).

In formula 1 the U_3 has been subtracted from U_1 to decouple the translational and rotational vibrations of the molecule. Because of the circular trajectory of *Cp* atoms, the measured r distance is shorter than the true centroid-atom distance, R:

$$R = \sqrt{(U_3 - U_1)^2 + r^2} \quad (2)$$

A clear discontinuity in the magnitudes of angular amplitude $|\tau - 36°|$ at ~3.24 GPa, coincides with the unit-cell angle β crossing 90°, which testifies that the unit-cell anomalous compression and ring-atoms displacements are coupled. The atomic displacements in turn are due to the competition between the preferred eclipsed molecular conformation and the molecular close-packing in the crystal structure. The phase transition of ferrocene at 165 K and the orthorhombic structure crystallized at 98 K both testify that the eclipsed conformation of *Cp* rings is favored in the isolated ferrocene molecule.[11,12,15,16] However, the symmetry of ferrocene monoclinic phase I would require that the molecule assumes the staggered conformation, with the *Cp* rings rotated angle by τ equal to 36°, corresponding to the potential energy (E_p) maximum. Consequently, the molecules become disordered and the *Cp* rings rotation angle τ changes between 23 and 49° on both sides of the E_p maximum. It is consistent with the direct observation of the disorder by neutrons and with large atomic displacements determined by the X-ray diffraction. For the isolated ferrocene molecule the E_p minimum lies at τ = 0° (eclipsed conformation), but the crystal environment of ferrocene I enforces a twisted conformation with the rings disordered. The double-well potential function corresponding to this disorder has the wells at angle τ of ~23° (i.e., 13° from the staggered conformation), as inferred from the amplitudes of atomic displacements (Figure 4) and structural refinements of the neutron-diffraction data.[10]

The low-temperature results show that the *Cp* rings vibrate dynamically between the two sites: below 165 K, this dynamics

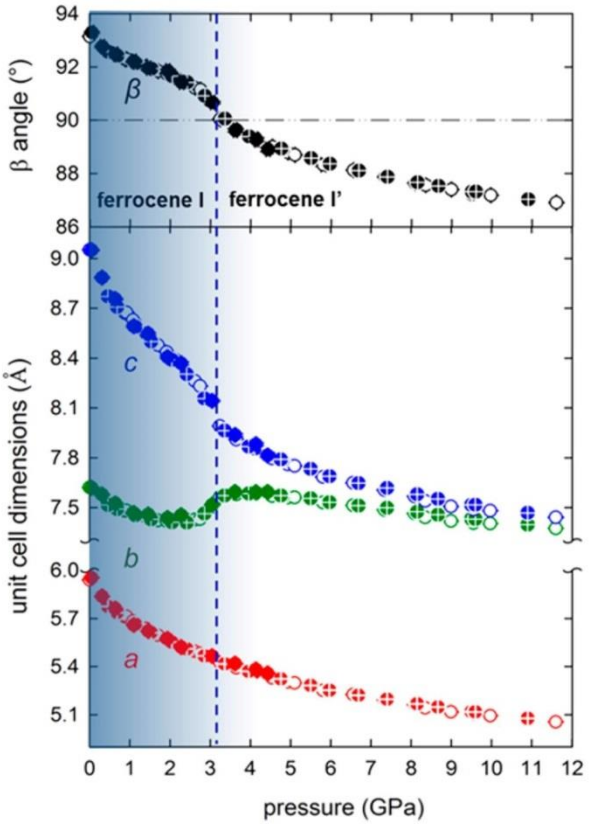

Figure 2. Compression of unit-cell dimensions of ferrocene up to 11.6 GPa. The vertical dashed line marks the transition between phases I and I′ at 3.24 GPa.

is frozen, which breaks the crystal symmetry to triclinic space group $P\bar{1}$. High pressure enhances the intermolecular interactions and acts similarly as low temperature in reducing the amplitudes of thermal vibrations but differently in that the confined space of the atomic vibrations is displaced away from the minima defined by the E_p double-well function of ambient pressure phase I. Thus high-pressure gradually enhances the crystal-environment forces, favoring the staggered conformation up to 3.24 GPa when the molecule locks in at the metastable position at τ equal to 36°. The enhanced environment effect is well-documented by the Raman signals of C−H vibrations increasingly separated by pressure (Figure 5).

The ferrocene crystal is strongly compressed, as expected for a molecular solid.[17] An element of this compression is that the enhanced intermolecular interactions reduce the *Cp* ring vibrations up to the point that only one well of the E_p function, molecular conformation and crystal environment contributions combined, has only one well, as illustrated in Figure 4. Owing to this one-well combined E_p function, the crystal acquires new properties and behaves differently at high pressure than at low temperature. Above 3.24 GPa, the crystal remains monoclinic, space group $P2_1/n$, but the molecules become ordered and truly centrosymmetric in the staggered conformation. The high-pressure suppression of the disorder present in ferrocene I as associated with the double-to-single well $E_p(\tau)$ function change is clearly reflected in the strongly anomalous unit-cell compression between 2.5 and 4.0 GPa and in the discontinuities of dc/dp and $d\beta/dp$ at 3.24 GPa. Thus the crystal undergoes an isostructural transition between phases I and I′ of the some translational and space-group symmetry. It is characteristic of such transitions that they are of the first-order type, according to Ehrenfest, and that they exhibit discontinuities in lattice parameters.[18]

The anomalous compression of ferrocene I can be explained by the mechanism involving the compression of intermolecular contacts and eliminating the disorder summarized below. Between 0.1 MPa and 3.24 GPa, the tightening contacts between *Cp* rings confine their range of vibrations and push the molecules into the metastable ordered conformation, as previously described (Figure 4). Above 3.24 GPa, the crystal compression cannot be further absorbed by the conformational changes, and the crystal transformations proceed toward equal intermolecular distances. It can be seen in Figure 6 that the intermolecular distance $d[111]$ along diagonal $[111]$ is shorter than $d[-111]$ along diagonal $[-111]$; therefore, the lattice strain proceeds toward angle β equal to 90° when both of these distances become equal. In the third stage above 4.0 GPa, the distances between ferrocene molecules are approximately equal (these differences are negligible compared to the anisotropic dimensions), and the structure resumes the positive compression.

This mechanism of compression also affords the explanation of the β-angle and *c*-length compression discontinuities (Figure

dx.doi.org/10.1021/jz402254b | *J. Phys. Chem. Lett.* 2013, 4, 4032−4037

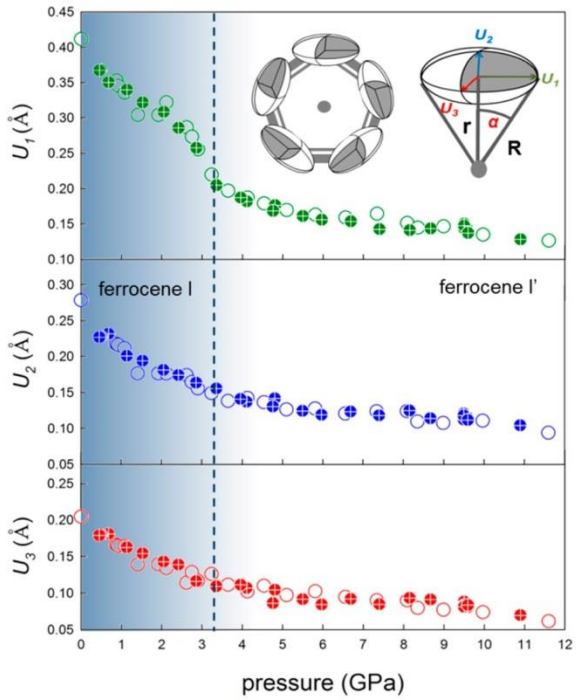

Figure 3. Pressure dependence of the principal semiaxes of the vibrational ellipsoid of carbon atoms in the *Cp* ring of ferrocene I. Semiaxis U_1 is tangential to the ring, U_2 is radial, and U_3 perpendicular to the ring. The plotted points are averaged for five symmetry-independent atoms C1−C5.

2). The pressure, where distances along [111] and [−111] become equal (Figure 6), clearly correlates with the damping of *Cp* rings vibrations (Figure 3). Thus at 3.24 GPa the crystal becomes ordered (Figure 5), which coincides with the equal Fe···Fe distances and the β angle equal to 90°.

The compilation of pressure-induced compression of d[111] and d[−111], as a combination of compression of the crystal in the (101) plane and along [010], explains the U-turn observed in the $b(p)$ function. In the process of adjusting, the d[111] and d[−111] distances are the strongest in plane (101), and parameter b clearly absorbs some of the changes (Figure 6). It is amazing that several critical transformations of the C-atoms displacements, d[111] and d[−111] distances becoming equal and the β-angle crossing the 90° value, coincide and have discontinuous character, consistently with transformations between isostructural phases. Hence, new phase I′ has been assigned to ferrocene above 3.24 GPa. Owing to the anisotropic molecular shape and to the tilts of the molecules, the crystal symmetry cannot be increased to orthorhombic or tetragonal system and the compression of the structure continues in the monoclinic system, with the β angle assuming acute values.

It should be noted that the U-turn compression of crystal parameters was observed for other compounds, too, although it was not connected to isostructural phase transitions.[19,20] It appears that the U-turn compression of crystal dimensions can be quite common, and presently we have provided its first description for this type of transformation for ferrocene. In general, the transformation between ferrocene I and I′ can be classified as an isostructural phase transition, which requires that the space-group symmetry of both phases remains the same and that the dimensions of the unit cell are only modified (no cell doubling or reconstruction takes place). Such isostructural transformations were observed for many crystals, for example, 1,3-cyclohexanedione,[21] sucrose,[22] sulfamic acid,[23] and, potassium titanyl phosphate (KTP).[24] A general description of such phase transitions within the Landau's theory was presented,[25] but it imposes no conditions on the crystal compression, apart from the fact that the transition is discontinuous. In our measurements, no discontinuity of crystal volume was detected, but discontinuities in the unit-cell parameters c and β were noted. It is known that discontinuity in volume at isostructural phase transitions decreases with pressure and disappears at the critical point (it is the tricritical point generally for first-order phase transitions) in the supercritical region of the phase diagram. It is thus plausible that the observation of the transition in ferrocene proceeds close to the critical point, the discontinuity effect in the volume is very subtle, or the new feature of the phase transition between ferrocene I and I′, that molecules are enforced by pressure to assume the conformations metastable under normal conditions (as opposed to the Gibbs free-energy shapes considered for the isostructural phase transitions[25]), does not require a discontinuity in volume.

It can be concluded that ferrocene I undergoes a pressure-induced isostructural transition to phase I′. This transition is unique in this respect that in the double-well potential of phase I the dynamics of the molecular rings is confined by pressure to the metastable position and that this process is coupled to the lattice dimensions in a U-turn dependence of parameter b. This anomalous dependence of b compensates the strain of intermolecular interactions in the crystal. The mechanism of the pressure-induced phase transition in ferrocene is fully consistent with the extensive experimental information about transformations and polymorphism of ferrocene at ambient

dx.doi.org/10.1021/jz402254b | *J. Phys. Chem. Lett.* 2013, 4, 4032−4037

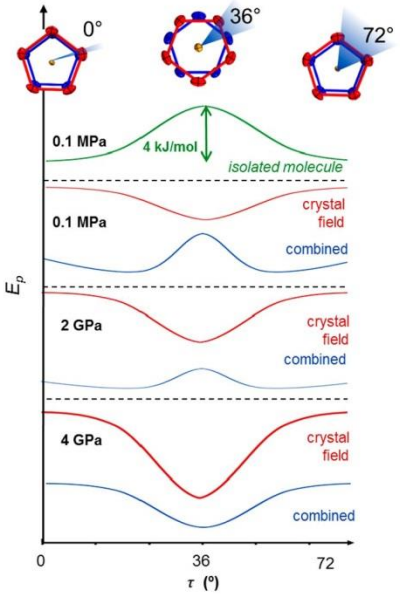

Figure 4. Conformations of isolated ferrocene molecule projected down its C_5 axis: eclipsed ($\tau = 0°$) and staggered ($\tau = 36°$) as well as the potential energy (E_p) of the conformers as a function of τ according to theoretical calculations and spectroscopic results[15,16] (green plot). Red plots represent the effect of crystal field, gradually enhanced with increasing pressure, and blue plots show its combination with the conformational energy (green) and the increasing contributions of the crystal field.

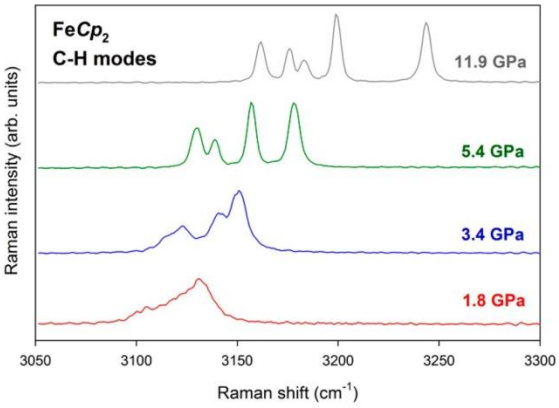

Figure 5. Vibrational C−H modes in the Raman spectra of compressed ferrocene at 1.8, 3.4, 5.4, and 11.9 GPa.

pressure and provides further understanding of the structural features and properties of this prototypic compound.

■ EXPERIMENTAL SECTION

Laboratory Data. A series of high-pressure diffraction experiments with a diamond anvil cell (DAC) have been performed. A modified Merrill−Basset DAC[26] and steel gaskets, 0.15 mm thick with 0.45 mm diameter hole, were used. Two methods of preparing the sample crystal were applied. In the first approach, a single crystal of ferrocene and a small ruby chip were glued to

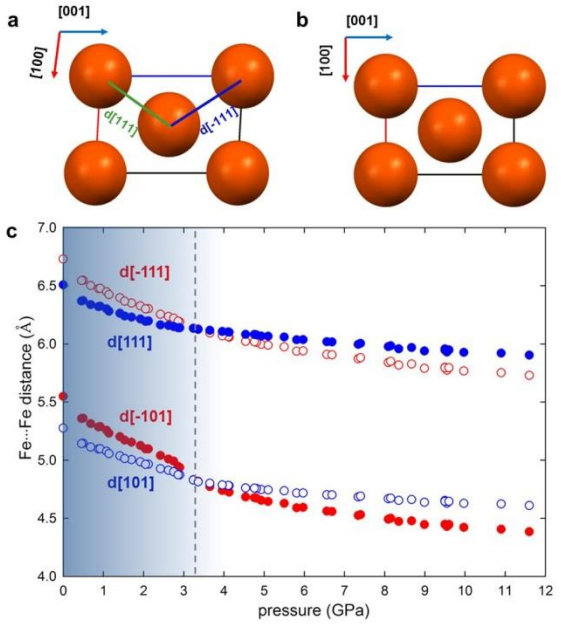

Figure 6. Schematic illustration of the ferrocene I and I′ structure (a) at 0.1 MPa; and (b) at 3.24 GPa when both distances $d[111]$ and $d[-111]$ are equal and the monoclinic angle β becomes equal to 90°. (The molecules are represented by large spheres.) Distances between the molecule centroid (Fe atoms) along crystal directions [111] and [−101] are plotted in panel c. Pressure dependence of distances $d[111]$ and $d[-111]$ is considerably weaker than that for the projections of the intermolecular vectors down the [010] axis and shown as the $d[101]$ and $d[-101]$ distances, respectively.

the culet surface of a diamond anvil, covered by steel gasket, and filled by methanol/ethanol/water hydrostatic liquid (vol. 16:3:1). In the second approach, a single crystal was in situ grown under high-pressure conditions. The chamber was filled by polycrystalline ferrocene and hydrostatic mixture. The isochoric in situ crystallization was performed at 0.33 GPa. Pressure in the DAC was calibrated by ruby fluorescence method and each time gradually increased before the diffraction measurements. Then, the DAC was mounted on the diffractometer and aligned using a gasket-shadow centring procedure. The CrysAlisPro program suite was used for data collection, determination of the UB matrices, and initial data reduction. Finally, the reflection intensities were corrected for the DAC absorption and gasket shadowing,[27,28] and the diamond-anvil reflections were eliminated. All of the ferrocene crystal structures were solved and refined using SHELXS and SHELXL programs.[29] Hydrogen atoms were located from geometry after each refinement cycle with $U_{iso} = 1.2U_{eq}$ of their carriers.

Synchrotron Data. High-pressure diffraction experiments have been performed at ID09A synchrotron beamline (ESRF) using parallel monochromatic X-ray beam ($E = 30$ keV, $\lambda = 0.413$ Å) focused to 15 × 10 μm^2 on the sample. We used a membrane-driven high-pressure cell equipped with Boehler-Almax seats and diamond-anvil design, allowing an opening cone of 64°. The culet size was 600 μm,and the sample was loaded together with He as pressure transmission medium into a hole in a stainless-steel gasket preindented to ∼0 μm with an initial

dx.doi.org/10.1021/jz402254b | J. Phys. Chem. Lett. 2013, 4, 4032−4037

diameter of 250 μm. Single-crystal data have been collected by a vertical-acting ω-axis rotation with an integrated step scan of 0.5° and a counting time of 1 s per frame. Diffraction intensities have been recorded with a Mar555 flat-panel detector. Diffraction data have been processed and analyzed with CrysAlisPro-171.34.44 software. Experimental data have not been corrected for absorption cause of the high energy of the X-ray beam. Frames have been rescaled using Friedel diffraction pairs to correct for variable diffracting volume as function of ω position. Pressures were measured with the Ruby fluorescence method using the nonlinear hydrostatic calibration by Mao et al. Raman spectra were collected with a micro optical system, equipped with notch filters, a HR460 spectrograph (Jobin Yvon) with a 1200 lines/mm grating, and a Pelletier-cooled CCD-detector. The excitation wavelength was 532 nm (green frequency-doubled NdYag laser), and the laser power was limited to ~10 mW.

■ ASSOCIATED CONTENT

Supporting Information

Experimental procedures and structural details of ferrocene crystals. This material is available free of charge via the Internet at http://pubs.acs.org. CCDC 960861−960911 contains the supplementary crystallographic data for 50 high-pressure measurements (respectively, from 0.0001 to 11.6 GPa) of ferrocene crystals. These data can be obtained free of charge from the CCDC via www.ccdc.cam.ac.uk/data_request/cif.

■ AUTHOR INFORMATION

Corresponding Author

*E-mail: katran@amu.edu.pl.

Notes

The authors declare no competing financial interests.

■ ACKNOWLEDGMENTS

The study was supported by the TEAM Programme of the Foundation for Polish Science, grant 2009-4/6.

■ REFERENCES

(1) Kealy, T. J.; Pauson, P. L. A New Type of Organo-Iron Compound. *Nature* **1951**, *168*, 1039−1040.
(2) Pauson, P. L. Ferrocene − How it all Began. *J. Organomet. Chem.* **2001**, *637*−*639*, 3−6.
(3) Werner, H. At Least 60 Years of Ferrocene: The Discovery and Rediscovery of the Sandwich Complexes. *Angew. Chem., Int. Ed.* **2012**, *51*, 6052−6058.
(4) Kauffman, G. B. The Discovery of Ferrocene, the First Sandwich Compound. *J. Chem. Educ.* **1983**, *60*, 185−186.
(5) Long, N. J. *Metallocenes: Introduction to Sandwich Complexes*; Wiley-Blackwell: London, U.K.; 1998.
(6) Seiler, P.; Dunitz, J. The Structure of Nickelocene at Room Temperature and at 101 K. *Acta Crystallogr., Sect. B* **1980**, *36*, 2255−2260.
(7) Robin, D.; Rogers, R. D.; Atwood, J. L.; Foust, D.; Rausch, M. D. Crystal Structure of Vanadocene $(\eta^5\text{-}C_5H_5)_2V$. *J. Cryst. Mol. Struct.* **1981**, *5*−*6*, 183−188.
(8) Bunder, W.; Weiss, E. Verfeinerung der Kristallstruktur von Dicyclopentadienyl-Magnesium, $(\eta^5\text{-}C_5H_5)_2Mg$. *J. Organomet. Chem.* **1975**, *1*, 1−6.
(9) Eiland, P.; Pepinsky, R. X-Ray Examination of Iron Biscyclopentadienyl. *J. Am. Chem. Soc.* **1952**, *74*, 4971−4971.
(10) Takusagawa, F.; Koetzle, T. F. A Neutron Diffraction Study of the Crystal Structure of Ferrocene. *Acta Crystallogr., Sect. B* **1979**, *35*, 1074−1081.
(11) Seiler, P.; Dunitz, J. D. The Structure of Triclinic Ferrocene at 101, 123 and 148 K. *Acta Crystallogr., Sect. B* **1979**, *35*, 2020−2032.
(12) Seiler, P.; Dunitz, J. D. Low-Temperature Crystallization of Orthorhombic Ferrocene: Structure Analysis at 98 K. *Acta Crystallogr., Sect, B* **1982**, *38*, 1741−1745.
(13) Spackman, M. A.; Jayatilaka, D. Hirshfeld Surface Analysis. *CrystEngComm.* **2009**, *11*, 19−32.
(14) Karvaly, B.; Mallik, B.; Kemeny, G. Effects of Pressure on the Electrical Conductivity of Ferrocene. *J. Mater. Sci. Lett.* **1985**, *4*, 912−915.
(15) Coriani, S.; Haaland, A.; Helgaker, T.; Jørgensen, P. The Equilibrium Structure of Ferrocene. *ChemPhysChem* **2006**, *7*, 245−249.
(16) Haaland, A.; Nilsson, J. E. The Determination of the Barriers to Internal Rotations by Means of Electron Diffraction. Ferrocene and Ruthenocene. *Acta Chem. Scand.* **1968**, *22*, 2653−2670.
(17) Katrusiak, A. High-Pressure X-Ray Diffraction Studies on Organic Crystals. *Cryst. Res. Technol.* **1991**, *26*, 523−531.
(18) Jaeger, G. The Ehrenfest Classification of Phase Transitions: Introduction and Evolution. *Arch. Hist. Exact Sci.* **1998**, *53*, 51−81.
(19) Boldyreva, E. V.; Shakhtshneider, T. P.; Ahsbahs, H.; Sowa, H.; Uchtmann, H. Effect of High Pressure on the Polymorphs of Paracetamol. *J. Therm. Anal. Calorim.* **2002**, *68*, 437−452.
(20) Boldyreva, E. V.; Naumov, D. Yu.; Ahsbahs, H. Distortion of Crystal Structures of Some Co^{III} Ammine Complexes. III. Distortion of Crystal Structure of $[Co(NH_3)_5NO_2]Cl_2$ at Hydrostatic Pressures up to 3.5 GPa. *Acta Crystallogr., Sect. B* **1998**, *54*, 798−808.
(21) Katrusiak, A. High-Pressure X-Ray Diffraction Study on the Structure and Phase Transition of 1,3-Cyclohexanedione Crystals. *Acta Crystallogr., Sect. B* **1990**, *46*, 246−256.
(22) Patyk, E.; Skumiel, J.; Podsiadło, M.; Katrusiak, A. High Pressure (+)-Sucrose Polymorph. *Angew. Chem., Int. Ed.* **2012**, *51*, 2146−2150.
(23) Li, Q.; Li, S.; Wang, K.; Li, X.; Liu, J.; Liu, B.; Zou, G.; Zou, B. Pressure-Induced Isosymmetric Phase Transition in Sulfamic Acid: a Combined Raman and X-Ray Diffraction Study. *J. Chem. Phys.* **2013**, *138*, 214505.
(24) Allan, D. R.; Nelmes, R. J. The Structural Pressure Dependence of Potassium Titanyl Phosphate (KTP) to 8 GPa. *J. Phys.: Condens. Matter* **1996**, *8*, 2337−2363.
(25) Christy, A. G. Isosymmetric Structural Phase Transitions: Phenomenology and Examples. *Acta Crystallogr., Sect. B* **1995**, *51*, 753−757.
(26) Merrill, L.; Bassett, W. A. Miniature Diamond Anvil Pressure Cell for Single Crystal X-Ray Diffraction Studies. *Rev. Sci. Instrum.* **1974**, *45*, 290−294.
(27) Katrusiak, A. *REDSHABS, A Program for Correcting Reflections Intensities for DAC Absorption and Gasket Shadowing*; Adam Mickiewicz University: Poznań, Poland, 2003.
(28) Katrusiak, A. Shadowing and Absorption Corrections of Single-Crystal High-Pressure Data. *Z. Kristallogr.* **2004**, *219*, 461−467.
(29) Sheldrick, G. M. A short history of SHELX. *Acta Crystallogr., Sect. A* **2008**, *64*, 112−122.

Article A.3

D. Paliwoda, P. Wawrzyniak, A. Katrusiak,

Unwinding Au···Au bonded filaments in ligand-supported gold(I) polymer under pressure,

submitted

Unwinding Au···Au bonded filaments in ligand-supported gold(I) polymer under pressure**

*Damian Paliwoda,[a] Paulina Wawrzyniak[a] and Andrzej Katrusiak[a,]**

[a]*Faculty of Chemistry, Adam Mickiewicz University, Umultowska 89b, 61-614 Poznan (Poland)*
**e-mail: katran@amu.edu.pl*

Abstract: *The ultimately miniature insulated gold wires, single atom in diameter, of Au···Au bonded gold(I) diethyldithiocarbamate polymer, $AuEt_2DTC$, can be transformed depending on pressure and solvate contents. When synthesized in the presence of CH_2Cl_2, it crystallizes into a tetragonal $AuEt_2DTC{\cdot}xCH_2Cl_2$ phase α with Au···Au bonded filaments modulated into molecular Au_8-pitch helices. Low contents of CH_2Cl_2 favours the β phase, of ortho-rhombic space group Fddd and significantly reduces the volume. The α-$AuEt_2DTC{\cdot}xCH_2Cl_2$ crystal exhibits a highly unusual negative-area compressibility, due to the spring-like compression of helices, and above 0.05 GPa it transforms to phase β. In phase β, the helices extend their pitch to the Au_{16} interval and partly unwind their turn, which relaxes the tension generated by external pressure between neighbouring helices of the opposite handiness. This is a unique observation of atomic-scale helical filaments transformation, which otherwise is a universal process analogous to the helix reversal between DNA forms B and Z and to macroscopic unwind kinks in grapewine tendrils and telephone cords.*

The supramolecular architectures of metal organic frameworks (MOF's), two- and one-dimensional coordination polymers and metal complexes have been extensively studied due to their exceptional physical and chemical properties. These novel hybrid materials are required for various application involving gas storage and purification, catalysis, and ferroelectric switches.[1] Noble-metals complexes are particularly intriguing due to their closed-shell noble-metal interactions, strong luminescence and direct relevance to gold nanoparticles applied in medicine and technology. Such materials with metallophilic interactions exhibit fluorescent properties and are particularly suited in photochemical sensors.[2] Recently, several high-pressure studies on argentophilic and aurophilic interactions in noble-metals complexes were reported.[3] It was discovered that the luminescence of Au···Au bonded polymers based on gold(I) dithiocarbamates linked by oligomeric gold-gold interactions is highly piezo- and pyro-sensitive.[4] The luminescence shifts were associated with the compressed Au···Au distances and reduced HOMO-LUMO energy gap of neighboring gold(I) centers.

Here we report the pressure-induced shortening of aurophilic contacts in a gold(I) diethyldithiocarbamate polymer ($AuEt_2DTC$) and conformational transformations of this monoatomic gold filaments in the crystal structure. It is shown that its compression reduces differences between the DTC-ligand supported and unsupported Au···Au bonds. We have established that two known polymorphs of $AuEt_2DTC$, tetragonal α-phase,[5] space group $I4_1/a$, and orthorhombic β-phase,[6] space group *Fddd*, are low- and high-pressure forms of this compound with voids partly filled by CH_2Cl_2 molecules. Both the polymorphs are built of $[Au_2(C_4H_{10}NCS_2)_2]$ monomers linked into Au···Au bonded helical filaments (Figure 1). The transition between phases α and β involves molecular-scale transformations of the Au···Au filaments, their compression, changes of helical-modulation frequency and unwinding snags of their turns.

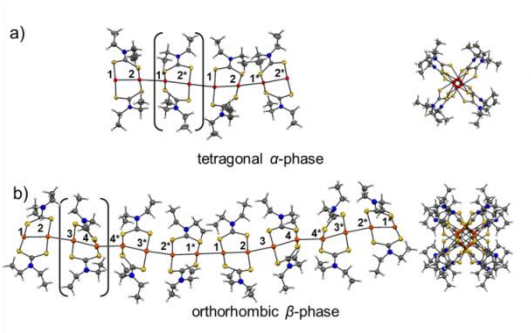

Figure 1. Single turns of helix-modulated Au···Au bonded filaments viewed perpendicular and along their direction in phases: (a) α-$AuEt_2DTC{\cdot}xCH_2Cl_2$; and (b) β-$AuEt_2DTC{\cdot}xCH_2Cl_2$. The $AuEt_2DTC$ monomer has been enclosed in brackets. The thermal ellipsoids are shown at the 30% probability level and isotropic H-atoms as small spheres.

We found that the formation of $AuEt_2DTC$ polymer forms α and β can be controlled at ambient pressure by the solvent mixture used for the synthesis and crystallization. The CH_2Cl_2:CH_3OH 1:1 mixture favours the formation of α-$AuEt_2DTC{\cdot}xCH_2Cl_2$, whereas of the solutions with a low contents of CH_2Cl_2, form β was obtained. It is also possible to obtain both forms together from one crystallization: initially form α precipitates, and then form β follows, when more volatile CH_2Cl_2 evaporated from the mixture, precipitates. We have associated the formation of phases α and β with the incorporation of CH_2Cl_2 molecules in the voids of $AuEt_2DTC$ crystals (Figure 2). Our single-crystal low-temperature and high-pressure structural studies confirmed the formation of solvated $AuEt_2DTC{\cdot}xCH_2Cl_2$, where *x* for different samples can assume values between ½ and 0. The guest CH_2Cl_2

molecules are strongly disordered in several orientations and their detection is hampered at room temperature by the adverse circumstances of very high atomic displacement parameters (ADP's) and very strong scattering of x-rays by Au atoms (relative electron density of other atoms is low). Additionally, the $AuEt_2DTC{\cdot}xCH_2Cl_2$ crystals are highly elastic and easily develop defects lowering the quality of single crystals. Our samples investigated at 0.1 MPa had x between 0.4 and 0.2 for phase α and for phase β x was close to 0. We have also substituted CH_2Cl_2 in the solvate mixture with CH_3OH by tetrahydrofuran (THF), the molecules of which are larger than the voids. The subsequent synthesis yielded exclusively the β-phase. The hydrophobic channels do not incorporate CH_3OH molecules. The solvation of $AuEt_2DTC$ by CH_2Cl_2 at ambient conditions results in the significantly larger, by nearly 10 $Å^3$, molecular volume (unit-cell V/Z) of phase α than that of phase β (see Figure 3 and Tables S1 and S2 of the Supplementary Information).

We further observed that above 50 MPa (0.05 GPa) the tetragonal crystals of α-phase transform to phase β, and that this transition is repetitively reversible, while the unsolvated orthorhombic β-phase crystals do not transform to phase α even after long time at ambient pressure, or after hydrostatic compression. The channel-like voids in $AuEt_2DTC$ have narrowings preventing transport of guest molecules to and out of the crystal. The CH_2Cl_2 molecules trapped in the voids are unlikely to be removed at normal conditions and reversely, high pressure do not push new guests into the voids. In principle, polymorphs should have the same composition. At ambient condition the $AuEt_2DTC{\cdot}xCH_2Cl_2$ forms α and β indicate their different solvation (larger x in form α and lower in β). On the other hand, the solvate of α form can be transformed to form β of the same composition by high pressure.

In both forms α and β the $Au_2(C_4H_{10}NCS_2)_2$ units polymerize into infinite Au···Au bonded filaments (Figure 1). We established that the crystal structures of forms α and β are closely related. Their unit-cell dimensions are correlated and have similar structures of the Au···Au bonded filaments. The filaments extend along crystal direction [001], as shown in Figure 2, and parameter c_β is approximately twice longer than c_α (the indices indicate forms α and β). Likewise, parameters a_α and b_α are approximately halves of the diagonals of the $a_\beta b_\beta$ unit-cell base. The CH_2Cl_2 solvate molecules 'inflate' the voids of phase α. These 'inflated' voids assume more spherical shape and the crystal assumes the tetragonal symmetry. Under high pressure the voids in the square pattern of filaments located in phase α collapse and are distorted toward a rhomboid pattern of phase β (Figure 2). This rhomboid pattern is also found for empty or on average nearly empty 'deflated' voids of unsolvated and hardly solvated $AuEt_2DTC{\cdot}xCH_2Cl_2$.

The crystal compression can be correlated to its structure built of Au···Au bonded helices and to the collapse of channel voids. The transformation between phases α and β hardly affects the distances between the close filaments (along directions $[100]_\alpha$ and $[010]_\alpha$ in phase α). In phase α these distances slightly increase with pressure along a_α and b_α, which leads to the negative-area compression of this phase. This effect can be compared to the increased radius of a compressed spring. The crystal discontinuous compression on the transition to phase β mainly results of collapsed voids, becoming longer along $[010]_\beta$ and shorter along $[100]_\beta$. This indicates that the interactions between neighbouring filaments are very important for the helical modulation of filaments. Owing to the similar parallel arrangement of the filaments, phase α is a prototypic ferroelastic form and phase β is its orientational state. The mechanism of collapsing voids in phase β leads to increasingly different parameters a_β and b_β with increasing pressure (Figure 3). The shorter parameter a_β is considerably softer than the longer b_β parameter. At still higher pressure the crystal gradually becomes more soft along $[010]_\beta$, however this direction remains the hardest in the crystal and at 1.0 GPa the difference between a_β and b_β increases to nearly 2.5 Å. Intramolecular Au···Au bonds within the $Au_2(C_4H_{10}NCS_2)_2$ monomers of 2.77-2.78 Å, are shorter than the Au···Au bonds between the monomers, of 2.96-3.01 Å at ambient conditions (Figure 4). In both phases the pitch of helix-modulated filaments is equal in length to the unit-cell c dimension, twice longer in phase β than in phase α (Figures 1 and 2). The strong compression of $AuEt_2DTC$ crystals along the Au···Au bonded helices parallel to the [z] axis (Figure 3) is the combined effect of both the compression of the Au···Au bonds (Figure 4) and to conformational transformations of the helices.

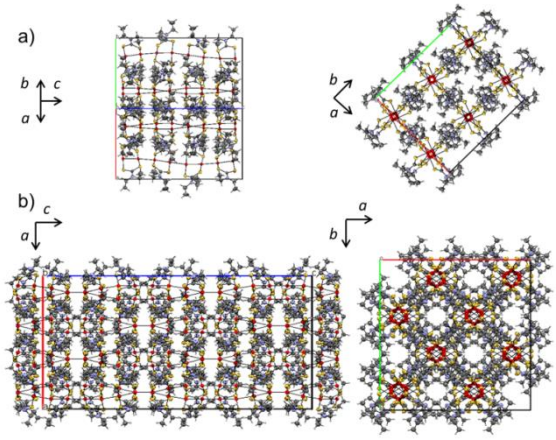

Figure 2. The crystal structure of $AuEt_2DTC{\cdot}xCH_2Cl_2$ viewed perpendicular to and along the Au···Au filaments: (a) phase α at 296 K / 0.1 MPa; (b) phase β at 296 K / 0.58 GPa. The thermal ellipsoids are drawn at the 50% probability level. The disordered CH_2Cl_2 molecules have been omitted for clarity (*cf.* Figure S7)

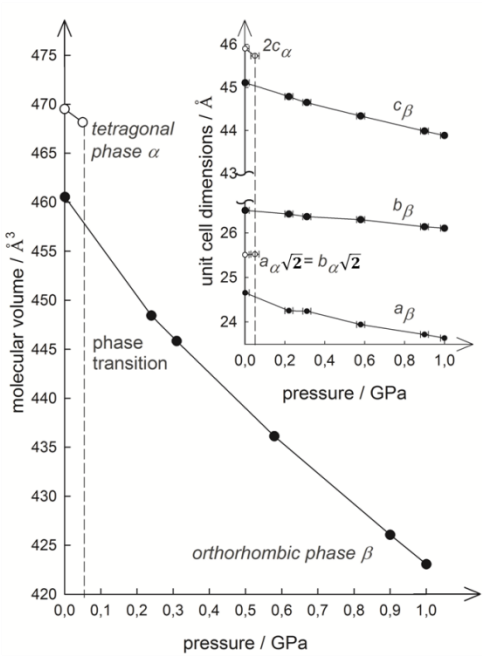

Figure 3. The pressure dependence of the unit-cell molecular volume(*V*/*Z*) of phases *α* (open circles) and *β* (full circles). Unit-cell parameters are shown in the inset. The dashed line indicates the transition pressure.

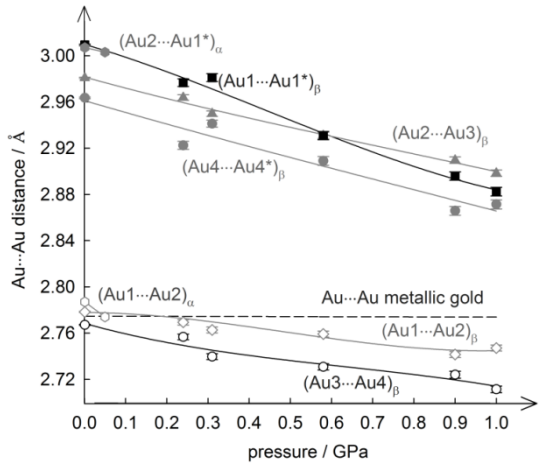

Figure 4. Compression of Au···Au distances in $AuEt_2DTC{\cdot}xCH_2Cl_2$ phases *α* (open circles) and *β* (full symbols): intramolecular ligand-supported bonds are shorter and intermolecular ligand-unsupported bonds are longer. The pressure dependence of Au···Au distance in compressed metallic gold[7] are shown as the dashed line.

The unsupported intermolecular Au···Au bonds are compressed at the average rate of β(Au···Au) = $(1/d)(\Delta d/\Delta p)$ equal to -0.1006 GPa^{-1}. The intramolecular ligands-supported Au···Au bonds are more than twice harder and their average β(Au···Au) is -0.0435 GPa^{-1}, measured between 0.1 MPa and 1.0 GPa. At 0.1 MPa, the supported Au···Au bonds are similar in length to those in metallic gold. Pressure of 1.0 GPa squeezes these supported Au···Au distances on average to the distance by 0.05 Å shorter than that in metal; the difference between unsupported Au···Au bonds and metallic gold is reduced from 0.2 Å at 0.1 MPa to 0.1 Å. The Au_8 turn of the helix in phase *α* is quite regular, according to two symmetry-independent Au···Au···Au···Au torsion angles equal to -45˚ (Figure 5 and Figure S1 in the Supplementary Information). In *β*-$AuEt_2DTC{\cdot}xCH_2Cl_2$ the Au_{16}-pitch helices become less regular (Figure 5). Phases *α* and *β* are centrosymmetric and there are both left- and right-handed helices. The helical modulation can be connected with the intramolecular and intermolecular strain between the Et_2DTC units. Annular S-Au-Au angles inside the $AuEt_2DTC$ monomers are between 81.4 and 95.2°. The annular torsion angles S-Au-Au-S are on average -37°, and extra-annular ones of about -63° (Figure S1). The compression of phase *α* increases the annular S-Au-Au-S angles and decreases the extra-annular ones by about 5°. The Au-Au-Au angles are of about 171° and 177°, which illustrates the directional flexibility of Au···Au bonds and their sensitivity to the crystal environment. Despite the similar structure of phases *α* and *β*, the ligands are considerably shifted, according to the changed modulation of filaments.

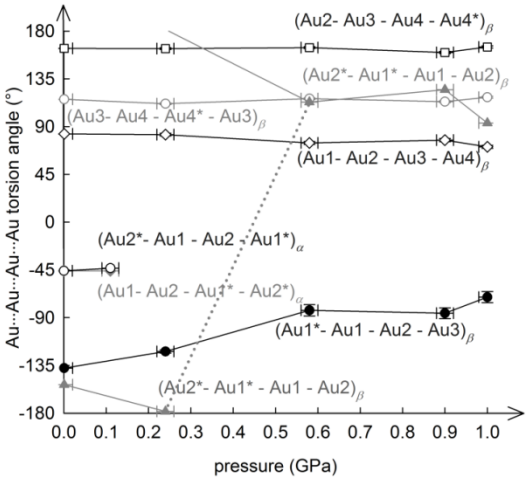

Figure 5. Torsion angles Au-Au-Au-Au as a function of pressure in *α*-$AuEt_2DTC$ (open circles) and in *β*-$AuEt_2DTC$ (full circles).

This modulation change can be rationalized by increased interactions between neighbouring filaments. In phase *α* their helix modulation is of the opposite handiness, as illustrated in Figure 6. The opposite handiness of helices is unfavorable for close packing, as the threads cannot efficiently fit into the grooves running in the opposite sense.[8] The close packing can be improved when the turns at least partly reverse their handiness, as observed in the *β* phase (Figure 5).

It can be concluded that at ambient conditions the Au···Au bonded polymer, $AuEt_2DTC{\cdot}xCH_2Cl_2$ crystallizes in forms *α* and *β*, depending on the contents (*x*) of solvating CH_2Cl_2 in the hydrophobic voids. Form

α is favoured by larger contents of CH_2Cl_2, whereas its lower content leads to phase β, with the smaller voids and the filaments around more tightly packed than in phase α. The high solvation causes a loose packing of filaments and their helical modulation in α-$AuEt_2DTC{\cdot}xCH_2Cl_2$. In the high-pressure β-form the frequency of filaments is halved and unwinding snags develop, which facilitate a tighter accommodation of helices of opposite handiness. The effect of large CH_2Cl_2 contents 'inflating' the voids in the α-$AuEt_2DTC{\cdot}xCH_2Cl_2$ can be counteracted by pressure, inducing the transition to phase β at about 50 MPa. The transition pressure value hardly depends on the solvent-content parameter x, fixed during the synthesis and can be tuned by this parameter Owing to this feature $AuEt_2DTC{\cdot}xCH_2Cl_2$ is an attractive material for pressure sensors, particularly as this compound is built of metallic Au···Au filaments. Their modulation is, to our knowledge, the smallest-scale observation of a helix, changing its frequency and partly unwinding. These transformations can be rationalized in the terms of pressure-enhanced interactions in the crystal lattice, and also correlated with the solvate contents. In these respects the transformations of helical filaments in $AuEt_2DTC{\cdot}xCH_2Cl_2$ resemble those of DNA and RNA helices.

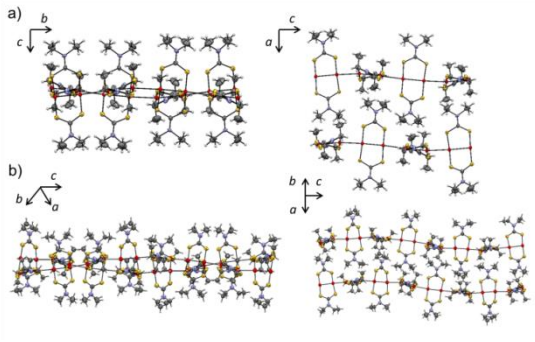

Figure 6. The closest filaments with their ligands mashed in the structure of $AuEt_2DTC{\cdot}xCH_2Cl_2$ viewed along (left) and perpendicular (right) to their average planes in: (a) phase α; and (b) phase β. The handiness of each helix is opposite to that of its four closest neighbours (*cf.* Figure2).

The mother-liquor composition and high pressure are known to induce transformation between left and right-handed helices in DNA forms *B* and *Z*,[9] respectively, and between the opposite-handiness helices in RNA forms *A* and *Z*.[10] Several elements of the filaments transforming in $AuEt_2DTC{\cdot}xCH_2Cl_2$ are consistent with the characteristic features in the mathematical model of unwinding snags describing macroscopic systems,[11] such as climbing-plants tentacles and telephone cords. The copmpression of Au···Au distances indicate that high-pressure synthesis of aurophilic complexes can lead to new compounds of ligand supported monoatomic wires.

Experimental Section

Synthesis of sodium diethyldithiocarbamate trihydrate.
Sodium diethyldithiocarbamate trihydrate was synthesized according to the previously described procedure.[12] 5.15 ml of diethylamine (50 mmol) in 15 ml of methanol and 2 g of sodium hydroxide (50 mmol) dissolved in 5 ml of distilled water were mixed together in a 50 ml Erlenmeyer flask. The mixture was cooled in the ice bath and stirred. Through a dropping funnel 3 ml (50 mmol) of carbon disulfide in 15 ml of methanol was carefully added to the mixture drop by drop. After 30 minutes the pale-yellow powder precipitated. The resulting precipitate was filtered off on a Büchner funnel, washed with distilled water and left to dry. Yield 67%.

Synthesis of gold(I) diethyldithiocarbamate polymer $AuEt_2DTC$.
Gold(I) diethyldithiocarbamate polymer $[Au_2(C_4H_{10}NCS_2)_2]_n$ was synthesized in the reaction of sodium diethyldithiocarbamate trihydrate with PPh_3AuCl gold(I) complex (from Sigma-Aldrich without further purification) in the dichloro-methane/ methanol (v:v / 1:1) solution. 0.1 g of PPh_3AuCl dissolved in 2 ml of dichloromethane was added to a 2 ml methanol solution of sodium diethyldithiocabamate. The resulting mixture was stirred for 8 hours until colourless crystals of triphenylphosphine precipitated. The precipitate was filtered off and the solution was left for crystallization. After one day needle-like orange crystals formed in the mother-liquor.

High pressure x-ray structural studies of $AuEt_2DTC$.
X-Ray diffraction measurements of gold $AuEt_2DTC$ needle-like single crystals were performed using diffractometers KUMA KM4 and Oxford Diffraction Xcalibur Eos equipped with a CCD detector and a monochromated Mo sealed tube source (Kα radiation, λ=0.71073 Å). For high pressure experiments a modified Merrill-Bassett diamond-anvil cell[13] (DAC with the anvils mounted directly on the steel supports) was used. A single crystal of gold(I) complex and a small ruby chip were glued to the culet surface of a diamond anvil. A tungsten gasket 0.1 mm thick and with 0.3 mm diameter hole was mounted. The chamber was filled with methanol used as a hydrostatic medium and closed. The DAC was centered on the diffractometer by the semiautomatic gasket-shadow procedure.[14] The CrysAlisPro program suite was used for the data collection, UB-matrix determination and initial data reduction. Then the reflections intensities were corrected for the DAC absorption and gasket shadowing and diamond-anvil reflections were eliminated. The high pressure x-ray experiments were performed at 0.24, 0.58, 0.90 and 1.0 GPa. Because of long unit-cell parameter c exceeding 45 Å the sample-detector distance was increased to 110 mm which optimized the experimental conditions between x-rays absorption in air, coverage of recorded data by more distant detector and the resolution of closely located reflections. Another difficulty associated with the large lattice constants was the considerable number of densely distributed sample reflections of which many overlapped with the reflections from the diamond anvils. Hundreds of so overlapped reflections have been scrupulously eliminated. The structures were solved and refined using SHELX programs.[15] Structural and experimental details are available free of charge in the CIF format from the Cambridge Crystallographic Database Centre.

****** This study was supported by the TEAM grant of the Foundation for Polish Science, TEAM 2009-4/6.

Keywords: gold polymers • aurophilic interactions• phase transition • micro-wires • compressed helices

[1] a) L. R. MacGillivray, R. H. Groeneman, J. L. Atwood, *J. Am. Chem. Soc.* **1998**, *120*, 2676-2677; b) M. Yaghi, G. Li, *Angew. Chem. Int. Ed.* **1995**, *34*, 207-209; c) T. Lasanta, M. E. Olmos, A. Laguna, J. M. Lopez de Luzuriaga, P. Naumov, *J. Am. Chem. Soc.* **2011**, *133*, 16358-16361; d) H. Li, M. Eddaoudi, T. L. Groy, O. M. Yaghi, *J. Am. Chem. Soc.* **1998**, *120*, 8571-8572; e) J. Lee, O. K. Farha, J. Roberts, K. A. Scheidt, S. T. Nguyen, J. T. Hupp, *Chem. Soc. Rev.* **2009**, *38*, 1450-1459; f) T. P. Vaid, E. B. Lobkovsky, P. T. J. Wolczanski, *J. Am. Chem. Soc.* **1997**, *19*, 8742-8743; g) L. H. Gade, *Angew. Chem. Int. Ed.* **1997**, *11*, 1171-1173.

[2] H. Schmidbaur, *Gold Bull*. **2000**, *33*, 3-10.

[3] a) A. B. Cairns, J. Catafesta, C. Levelut, j. Rouquette, A. van der Lee, L. Peters, A. L. Thompson, V. Dimitriev, J. Haines, A. L. Goodwin, *Nature Materials* **2013**, *12*, 212-216; b) A. L. Goodwin, D. A. Keen, M. G. Tucker, Proc. Nat. Acad. Sci. USA 2008, *105*, 18708-18713; c) J. M. Ogborn, I. E. Collings, S. A. Moggach, A. L. Thompson, A. L. Goodwin, *Chem. Sci.* **2012**, *3*, 3011-3017.

[4] F. Baril-Robert, M. A. Radtke, C. Reber, *J. Phys. Chem. C* **2012**, *16*, 2192-2197.

[5] D. D. Heinrich, J.-V. Wang, J. P. Fackler, *Acta Crystallogr. Sect. C* **1990**, *46*, 1444-1447.

[6] M.-C. Hong, X.-J. Lei, Z.-Y. Huang, B.-S. Kang, F.-l. Jiang, H.-Q. Liu, *Chin. Sci. Bull.* **1993**, *38*, 912-915.

[7] M. Matsui, *J. Phys.* **2010**, *215*, 012197.

[8] M. Podsiadło, E. Patyk, A. Katrusiak, *CrystEngComm* **2012**, *12*, 6419-6423.

[9] A. Krzyżaniak, P. Sałański, J. Jurczak, J. Barciszewski, *FEBS Lett.* **1991**, *279*, 1-4.

[10] A. Krzyżaniak, J. Barciszewski, J. P. Fürste, R. Bald, V. A. Erdmann, P. Sałański, J. Jurczak, *Int. J. Biol. Macromol.* **1994**, *16*, 159-162.

[11] a) A. Goriely, m. Tabor, *Phys. Rev. Lett.* **1998**, *80*, 1564-1567; b) S. Przybył, P. Pierański, *Eur. Phys. J.* **2001**, *E4*, 445-449; c) P. Pierański, J. Barańska, A. Sklejtorp, *Eur. J. Phys.* **2004**, *25*, 613-621.

[12] A. Hulanicki, *Talanta* **1967**, *14*, 1371-1392.

[13] L. Merrill, W. A. Bassett, *Rev. Sci. Instrum.* **1974**, *45*, 290-294.

[14] A. Katrusiak, *Z. Kristallogr.* **2004**, *219*, 461-467.

[15] G. M. Sheldrick, *Acta Crystallogr. Sect. A* **2008**, *64*, 112-12

11
Appendix B

Compressibility of solids in a piston-cylinder apparatus

The compressibility of imidazole has been measured in a piston-cylinder apparatus. For measuring the compressibility of this solid compound a hydrostatic fluid had to be used. For this purpose kerosene (from Dragon without further purification) was chosen. The compressibility of kerosene is essential for retrieving the compressibility of the solid component in the chamber. The compressibility measurements of kerosene performed in the piston-cylinder apparatus are plotted in Figure B.1 and reported in Table B.1. The initial volume of kerosene sample was 9.8 ml.

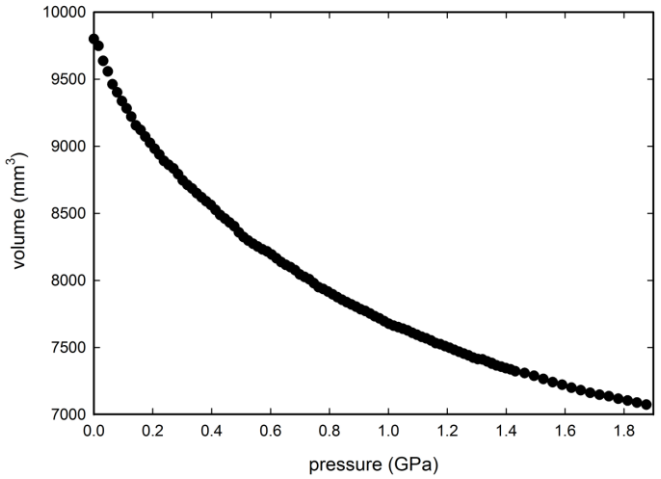

Figure B.1. *Compressibility of kerosene.*

Table B.1. *Compressibility data of kerosene.*

pressure (GPa)	volume (mm^3)	pressure (GPa)	volume (mm^3)	pressure (GPa)	volume (mm^3)	pressure (GPa)	volume (mm^3)
0.00	9800.00	0.45	8459.80	0.89	7803.83	1.34	7395.55
0.02	9747.98	0.46	8431.52	0.91	7784.61	1.35	7384.24
0.03	9636.01	0.48	8403.25	0.92	7772.16	1.35	7378.59
0.05	9557.97	0.49	8358.01	0.94	7752.94	1.37	7366.15
0.06	9461.84	0.51	8322.95	0.95	7732.58	1.38	7357.10
0.08	9401.90	0.52	8296.94	0.97	7716.75	1.40	7345.79
0.10	9336.30	0.54	8273.19	0.99	7696.39	1.42	7336.74
0.11	9282.01	0.56	8251.70	1.00	7677.16	1.43	7323.17
0.13	9220.94	0.57	8231.34	1.02	7662.46	1.46	7309.60
0.14	9155.35	0.59	8216.64	1.03	7651.15	1.49	7289.24
0.16	9121.42	0.60	8192.89	1.05	7639.84	1.53	7265.49
0.17	9072.78	0.62	8164.61	1.07	7627.40	1.56	7241.74
0.19	9025.28	0.64	8136.34	1.08	7609.30	1.59	7222.51
0.21	8981.18	0.65	8115.98	1.10	7594.60	1.62	7199.89
0.22	8938.20	0.67	8099.02	1.11	7579.90	1.65	7181.80
0.24	8890.70	0.68	8076.40	1.13	7567.46	1.69	7162.57
0.25	8861.29	0.70	8044.73	1.14	7552.76	1.72	7147.87
0.27	8834.15	0.72	8025.50	1.16	7532.40	1.75	7136.56
0.29	8792.30	0.73	8008.54	1.18	7524.48	1.78	7118.46
0.30	8745.93	0.75	7979.13	1.19	7509.78	1.81	7104.89
0.32	8712.00	0.76	7949.73	1.21	7497.34	1.84	7089.06
0.33	8684.86	0.78	7936.16	1.22	7482.64	1.88	7074.35
0.35	8649.80	0.80	7916.93	1.24	7467.93	1.91	7057.39
0.37	8619.26	0.81	7896.57	1.26	7454.36	-	-
0.38	8589.86	0.83	7875.08	1.27	7441.92	-	-
0.40	8562.72	0.84	7855.86	1.29	7424.96	-	-
0.41	8525.39	0.86	7837.76	1.30	7413.65	-	-
0.43	8486.94	0.87	7820.80	1.32	7411.38	-	-